Radio frequency sputter deposition of the transparent conducting wide band gap oxide Ga_2O_3

Dissertation

zur Erlangung des Doktorgrades der Naturwissenschaften

Doctor rerum naturalium

(Dr. rer. nat.)

vorlegt von

Philipp Schurig

angefertigt bei

PD Dr. Angelika Polity

Justus-Liebig-Universität Gießen

I. Physikalisches Institut

Gießen 2020

Abstract

Transparent conducting wide band gap oxides can be used in a variety of promising applications, e. g., thin film solar cells or transparent optoelectronic devices. Exemplary, a Cu_2O-based solar cell will represent a sustainable and non-toxic technology with the potential for affordable costs, if the chosen window layer materials also are sustainable and abundant. One suitable window layer material is Ga_2O_3 due to the favorable conduction band position relative to that of Cu_2O even though the growth of high quality material still is considered as rather difficult. However, by variation of deposition parameters, e. g. gas flows, sputtering power or substrate temperature, it is possible to specifically tailor the quality and properties of a deposited layer. Of major interest for commercialization of any technology is the capability for mass production. Thus, the conventional as well as pulsed-mode rf sputter deposition are favorable methods as they allow for industrial upscaling due to high deposition rates, excellent layer uniformity on large-area substrates and ease of automation. However, the latter is a new methodology whose parameter correlations and impacts have to be further investigated and explored. Preliminary studies have already shown the potential of this technology for reducing the allocated thermal energy during deposition while maintaining the same layer quality. In two consecutive publications, the feasibility of rf sputter deposition has been investigated, in conventional design as well as in pulsed-mode operation, in order to obtain Ga_2O_3 thin films of high quality.

In the first publication, the results of conventional rf sputter deposition of Ga_2O_3 by variation of the rf and heating power were discussed. A set of parameters yielding an optimized layer were found, though the quality was not sufficient for the utilization as a window layer material. Still, the thorough analysis of the results revealed a correlation which is very suitable for a fast determination whether the layer is grown stoichiometrically or not. The discrepancy between the refractive index dispersion of a layer and the respective bulk material can give a first impression about the compound's composition.

The second publication highlights the utilization of pulsed-mode rf sputter deposition for growing Ga_2O_3 layers. Slight improvements of layer quality were achieved but,

unfortunately, not yet good enough for targeting an application as functional layer in optoelectronic devices. Only a first impression of the complex relationship between conventional and new deposition parameters and their impact on the layer quality was obtained in these experiments. With increasing rf power and pulse duty cycle value, particle energies were accomplished which cannot be reached in conventional sputtering processes. Besides minor improvements in crystalline structure, another feature was identified which is tentatively assigned to growth of metastable γ-Ga_2O_3 at the interface between sapphire and Ga_2O_3 layer. An additional effect is suggested. The presence of negatively charged oxygen ions in the process leads to etching of the surface or penetrating into the layer inducing an increase of the optical band gap.

In conclusion, the results have revealed a new relationship for investigating layer stoichiometry only requiring optical measurement data. Furthermore, the experiment performed underlined the potential of the new growth methodology. The prospective exploration and understanding of the intertwined parameter spaces of conventional and pulsed rf sputtering bears great potential to overcome current obstacles in material research.

Contents

1 Introduction **1**

2 Application **3**

3 Transparent conducting oxide: Gallium sesquioxide **7**

4 Deposition of thin films **11**

5 Growth of β-Ga_2O_3 layers **15**

6 Summary and Outlook **21**

7 Publication Manuscripts and Contributions **23**
7.1 Publication 1 23
7.2 Publication 2 30

Bibliography **39**

Appendix **49**

A ZnMgO(:Al) **49**

B Annealing Ga_2O_3 **51**

Acronyms

Notation	Description
ALD	atomic layer deposition
CSD	chemical solution deposition
CVD	chemical vapor deposition
DFT	density-functional theory
HiPIMS	high-power impulse magnetron sputtering
HPPMS	high-power pulsed magnetron sputtering
MBE	molecular-beam epitaxy
PDC	pulse duty cycle
PLD	pulsed laser deposition
PRF	pulse repetition frequency
PVD	physical vapor deposition
rf	radio-frequency
RFG	radio-frequency generator
RSF	relative sensitivity factor
TCO	transparent conductive oxide
ToF-SIMS	time of flight secondary-ion mass spectrometry
XPS	X-ray photoelectron spectroscopy

CHAPTER 1

Introduction

Today, climate change is one of the world's pressing challenges and the quest to succeed with the energy transition towards renewable sources is ongoing. One small part of a possible solution is related to transparent conductive oxides (TCOs). These are of major interest for optoelectronic, high-power, sensor or energy-related devices [Gal18; Hig18; Hig16a; Hig16b; Ori00; Zin04]. They are already an indispensable component of many present technologies, e. g. mobile phones, (electric) vehicles or photovoltaic cells. This material class combines low electric resistivity with high optical transmittance in the visible part of the electromagnetic spectrum. Especially of high interest are wide band gap materials which exceed a band gap size of 3 eV, i. e. are really transparent to visible light. Within a photovoltaic cell, the higher the band gap of the window layer, the larger is the fraction of the electromagnetic spectrum which reaches the absorber layer unhindered, and, thus, increases the conversion efficiency. Moreover, this topic is increasingly in the focus of research because of the depletion of fossil fuel resources, e. g. oil by 2044 [Sha09]. Therefore, the need for renewable energy sources as a substitute technology is even higher. According to the United Nations, the ratio of available solar energy to the worldwide energy consumption in the year 2050 (2100) is between 1.5–2.7 (0.8–1.8) up to 47–84 (26–57) [Age11; Nat01]. However, not to run the risk of material shortages one has to pay attention to the abundance as well as the criticality of materials used in corresponding devices such as solar cells. A list of critical materials and methodologies to identify and deal with these are provided by the European Union [Com17; Com20]. A promising compound as an absorber layer in solar cells seems to be the *p*-type cuprous oxide, Cu_2O. Although the predicted efficiency of 20 %, according to the Shockley-Queisser limit [Sho61], does not come off best, the abundance, sustainability as well as non-toxicity of the material and low-cost production, e. g. sputter deposition, compensate for this deficiency [Mey12]. The optimum window layer in a Cu_2O-based solar cell should possess an aligned conduction band or a small positive offset with respect to the absorber layer conduction band [Fon10]. One promising candidate is the thermodynamically most stable polymorph of the gallium sesquioxide, β-Ga_2O_3,

which exhibits already an almost ideal, slightly positively shifted, conduction band alignment with Cu_2O [Bra14; Min13b].
According to the EU list, and also the findings of A. Diederen in 2009, gallium must be considered critical whereas Cu is not [Die09]. The criticality of Ga mostly arises due to being only a by-product of the aluminum, copper or zinc production, which are all non-critical materials. However, the results of such criticality studies vary due to different methodologies weighing parameters such as geopolitical aspects, forecasted material reserves and so forth, differently.
Nevertheless, not only the availability of a material is important, but also the effort required to achieve material of high quality. In this context, the obstacles for Ga_2O_3 are rather high. State of the art material is obtained by crystal growth methods or molecular beam epitaxy [Pea18; Ste16]. As a consequence, thin films of high quality are predominantly available with small lateral sizes. Therefore, a reproducible large-scale deposition of Ga_2O_3 thin films by rf sputtering is of great technological interest for realizing Cu_2O-Ga_2O_3 solar cells. However, major obstacles are very high substrate temperatures or high condensing ion energies, both are needed to deposit single crystalline Ga_2O_3 material. A promising technique being able to reduce the growth temperature while maintaining high crystal quality is given by the DC sputtering technique of high-power pulsed magnetron sputtering (HPPMS) [Kel09; Sar10].

In this work, the methodology of a pulsed sputtering mode is combined with conventional radio frequency sputtering. However, the influence of the additional parameters, e. g. pulse duty cycle or pulse repetition frequency, on the basic parameters such as rf power, chamber pressure and gas fluxes were unknown. Thus, the interplay of these parameters, starting with the pulse duty cycle, was thoroughly investigated. With HPPMS it is possible to lower the substrate temperature and at the same time to increase the sputtering power while maintaining the layer quality. This allows a direct deposition of Ga_2O_3 onto the temperature sensitive absorber layer Cu_2O. The surface temperature needed for obtaining high quality crystalline Ga_2O_3 is shown to be much lower than that in a conventional sputtering ($> 500\,°C$) [Kum13; Ram14].

CHAPTER 2

Application

Manifold approaches for providing clean energy in the future exist with water, wind and solar energy harvesting technologies. Amongst the solar approaches are solar collectors and photovoltaic cells. Each technology has its own set of sub-technologies, e.g. photovoltaic cells can be divided into Si-based solar cells, die-sensitized or perovskite solar cells, thin film solar cells, and many more [Bag15]. However, especially within the group of thin film solar cells, many candidates contain rare or toxic materials, e. g., CdTe- or GaAs-based photovoltaic cells. Several worldwide conducted surveys and studies have identified various global megatrends which will rise in importance and impact in the future [Ber18a; Ber18b; Del17; KPM14]. Sustainability and energy efficiency are only two of them fostering the research of materials based on more abundant elements like Cu, Zn, or Mg.

First, to better analyze which combination of materials can satisfy the requirements for efficient photovoltaic cells the basic principle of the chosen technology will shortly be introduced. The key mechanism of solar cells relies on different types of semiconducting materials forming the required p-n junction. The depletion region of the pn-junction initially separates the charges generated by incident light via the present internal electrical field. Originating from the different functions in a photovoltaic cell the n- and p-type semiconductors go by the name of window and absorber layer, respectively. To avoid recombination of the separated charges both layers have to exhibit high electrical conductances for the respective minority charge carriers. At the same time their band gaps and band offsets have to be chosen correctly to fulfill their tasks as window or absorber layer to highest degree possible. Namely, a large band gap to allow as many photons as possible to pass unhindered through the window layer to reach the depletion region of the junction. There they will be absorbed by the absorber material generating free charge carriers, i.e. electrons and holes. One major obstacle in the search for suitable window layer candidates is due to the fact that wide band gap materials are often insulating. Furthermore, not only the individual properties of absorber and window layer are important for the performance of the solar cell, but also their energetic alignment at

the junction. For example, the conduction band offset between both layers strongly influences the major performance parameters of a solar cell, i.e. efficiency, fill factor, short circuit current as well as open circuit voltage, c. f. Fig. 2.1(b).

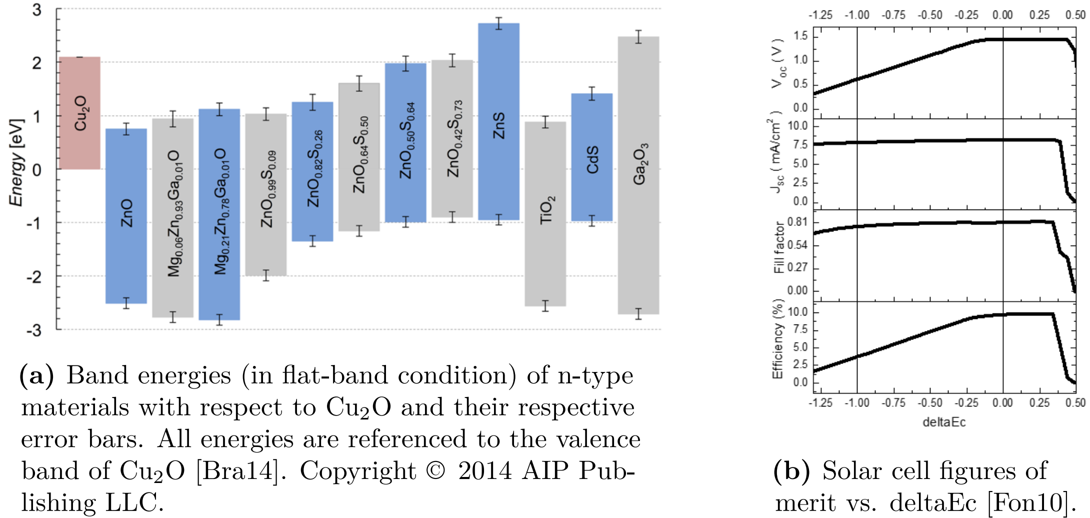

(a) Band energies (in flat-band condition) of n-type materials with respect to Cu_2O and their respective error bars. All energies are referenced to the valence band of Cu_2O [Bra14]. Copyright © 2014 AIP Publishing LLC.

(b) Solar cell figures of merit vs. deltaEc [Fon10].

Figure 2.1: Possible Cu_2O window layer candidates and figures of merit.

Consequently, possible combinations of layer materials have to be investigated in order to reveal whether their respective properties match each other. The focus of this work lies on the identification of a suitable window layer material in combination with the absorber material Cu_2O. Dicopper Oxide was chosen because it has long been a research focus for solar cells based on sustainable materials [Kra12; Mey12]. Brandt *et al.* [Bra14] have identified different n-type materials fulfilling, to varying degrees, the premise of a "small" conduction band offset, see Figure 2.1(a), of which CdS is not further addressed due to the toxicity of cadmium. The very well studied material ZnO and some related alloys are also part of the list. For example, T. Minami has shown that Al-doped ZnO is a promising material to replace tin-doped indium oxide (ITO), whose exponentially rising demand can no longer be satisfied at a reasonable price, and, thus triggers the quest for alternative TCO materials avoiding the element indium which is scarce and expensive. With regard to the critical material list of the EU, the elements Zn and Al are indeed seen as abundantly available [Com17; Com20]. Other very interesting elements for doping of ZnO, besides aluminum, are sulfur or magnesium as these enable extensive band gap engineering, 3.3 eV to 3.91 eV (ZnS, hexagonal) or 7.7 eV (MgO, cubic), respectively [Kro13; Roe67]. This allows for band gap engineering in semiconductor heterojunctions improving device efficiencies. For example ZnO_xS_y could be tuned to perfectly fit the conduction band offset. However, Tolstova *et al.* [Tol17] have shown that the interaction with the absorber material may result in the formation of an undesired interface material like the wide

band gap insulator $ZnSO_4$, representing the actual thermodynamically favorable compound formed of these elements. An increase in growth temperature leads to a reduction but not elimination of the presence of this parasitic zinc sulfate layer. This implies that the absorber layer stays intact. However, some additional challenges may arise, such as structural phase transformations above certain compositions, need of non-equilibrium growth methods to exceed the solubility limit, a strong reduction of electrical conductivity as well as criticality in case of Mg among others [Cho02; Com17; Min00; Oht98; Par01; Sar59; Seg65; Sun02]. Furthermore, from a technical point of view also preferential sputtering effects are another important factor to consider when choosing quaternary alloys for a sputter deposition process [Com17; Kel78]. The former was witnessed in preliminary studies (Appendix A) conducted by the author underlining that if intended for industrial utilization a co-sputtering approach of two distinct targets has to be chosen. It also should be noted that the rather rare Mg is used in many competing technologies, e. g. in the field of transportation or Al-alloy fabrication, thus, the supply risk is rather high.
Another candidate is TiO_2 with similar values for economic importance, supply risk [Com20] and conduction band offset. Unfortunately, the magnitude of the latter is similar as in case of ZnO and, thus yields comparable limitations with respect to efficiency [Kra12]. Therefore, the remaining and most promising n-type material for a window layer in Cu_2O-based photovoltaic cells seems to be gallium sesquioxide [Bra14; Min13a; Min13b], cf. Fig. 2.1. In this case, another beneficial influence on the solar cell performance should arise due to the positive conduction band offset between the absorber and window layer, i. e., with the conduction band of the latter being at a higher energy than that of the former [Fon10]. Ga_2O_3 is a binary material system and the problem of different sputtering yields, i.e. preferential sputtering, is not of utmost importance [Kel78] in sputter deposition processes as the incorporated oxygen can be replenished from the gas phase. Already in 2016, gallium was considered critical from the European Commission [Com20], since it cannot be mined directly and is a by-product and mainly recovered during Al or Zn processing. The forecast of supply and demand is only reliable until 2022 due to missing information from market or industry experts. Its natural abundance is much less than that of Zn and Al. Nevertheless, the supply risk of Ga is more governed by the industrial extraction capacity than by scarcity.

CHAPTER 3

Transparent conducting oxide: Gallium sesquioxide

For the first time the polymorphism and the five different phases α, β, δ, γ, and ε of the gallium oxide were mentioned and confirmed by Roy *et al.* [Roy52] in 1952, cf. Fig. 3.1. Still, more than 60 years later, many questions remain open. The aforementioned renewed interest in the material system is leading to great research efforts because of the broad spectrum of possible applications, especially for the most thermodynamic stable form β-Ga_2O_3 [Gal18; Pea18; Ste16; Wen17]. Therefore, only the β-phase of the gallium sesquioxide will be discussed in depth in what follows.

Bulk crystals of Ga_2O_3 can be either grown by melt or flux growth techniques [Åhm96; Gal10; Irm11]. Edge-defined film-fed growth for example is capable to produce single-crystal wafers with sizes from 2-inches up to 6-inches [Aid08; Kru18]. Thin films or nanostructures can be prepared by a variety of techniques: chemical vapor deposition (CVD) [Bat96], molecular-beam epitaxy (MBE) [Oku14; Reb02; Vil06; Vog16], pulsed laser deposition (PLD) [Mat06; Min13b], sol-gel synthesis [Min03; Moo11], sputtering [Mar12; Min03; Reb02], etc. The drawback of most of these techniques, e. g. MBE or PLD, is a low growth rate of only 0.09 [Osh07] or 0.22 $\mu m h^{-1}$ [Zha14], respectively. As a consequence, the growth rate of Ga_2O_3 thin films has to be increased in order for this kind of process to be of interest for industrial fabrication of devices. Almost all sputter-based techniques are suitable candidates for growing Ga_2O_3 thin films as their products are transferable to an industrial scale with only minor additional efforts. Post-deposition temperature treatments are also capable of increasing the layer quality after deposition [Aid14; Don16; Fen16]. Nevertheless, such temperature treatments should be avoided from an industrial point of view as the energy costs are huge. However, by reaching an annealing temperature of at least 870 °C under dry conditions, all other gallium oxide phases, if present, are transformed into the β-phase.

Crystallographic non-equivalent positions are one of many consequences of the monoclinic crystal structure of β-Ga_2O_3 , cf. Fig. 3.2 and Table 3.1. In detail, Ga atoms are either tetrahedrally coordinated Ga(1) or octahedrally coordinated

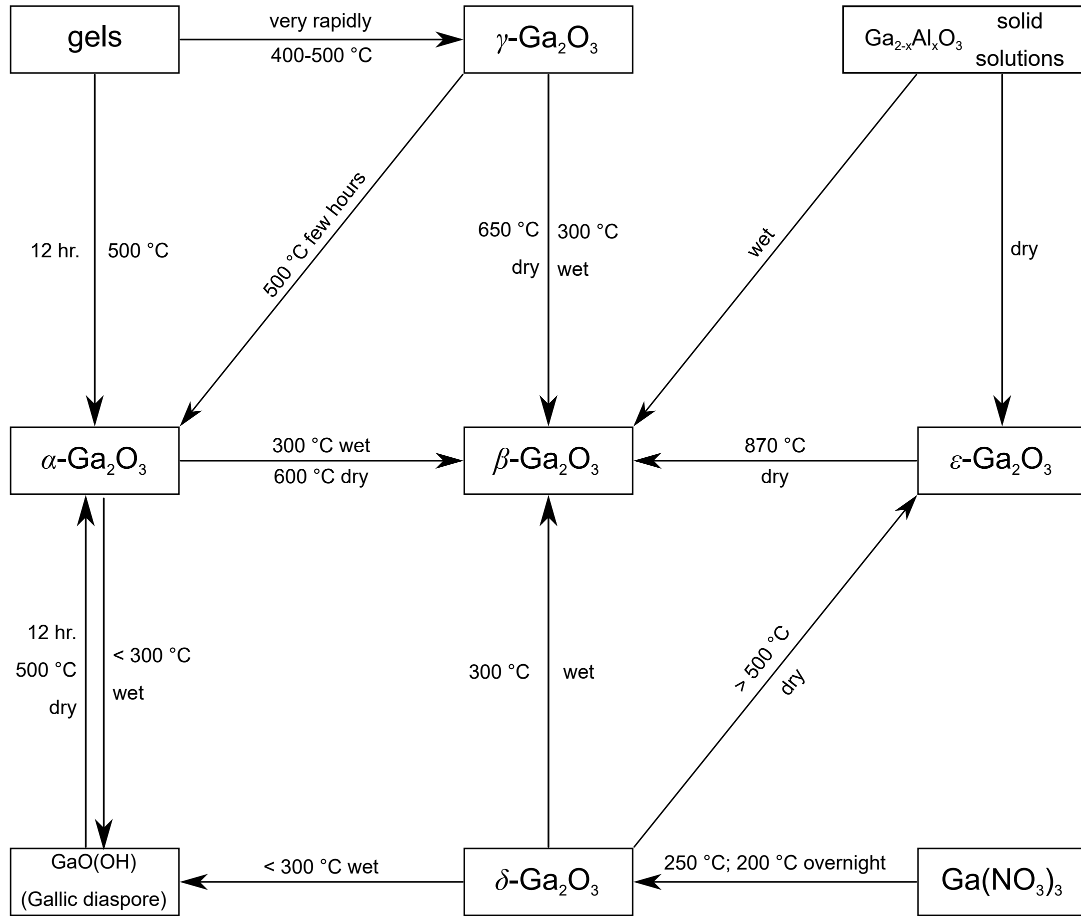

Figure 3.1: Temperature dependent transformation relations of Ga_2O_3 (after Roy et al. [Roy52])

Ga(2), whereas two of three oxygen atoms (O(1), O(2)) are trigonally coordinated and the remaining O(3) is tetrahedrally coordinated. The oxygen arrangement resembles a distorted cubic close-packed array [Ste16]. As a consequence of the low crystal symmetry Ga_2O_3 exhibits anisotropic properties, for example different thermal conductivities along different crystal directions, e. g. 29 W/mK along the [010] direction vs. 10.9 W/mK along the [100] direction [Guo15]. Furthermore, the electrical properties change from a conductivity of $38\,\Omega^{-1}\,\mathrm{cm}^{-1}$ and a mobility of $46\,\mathrm{cm}^2\,\mathrm{V}^{-1}\,\mathrm{s}^{-1}$along the b axis to $2.2\,\Omega^{-1}\,\mathrm{cm}^{-1}$ and $2.6\,\mathrm{cm}^2\,\mathrm{V}^{-1}\,\mathrm{s}^{-1}$for the c direction [Ued97]. Additionally, the optical properties strongly depend on the polarization of the impinging electromagnetic wave. The obtained Raman spectra depend heavily on the polarization direction and the investigated crystallographic plane [Kra16]. Similarly the absorption edge position differs for light with $E||b$ (4.79 eV) and with $E||c$ (4.52 eV) polarization [Ued97]. However, the electronic structure was

well investigated either by theoretical studies with density-functional theory (DFT) [Yam04; Yos07] or hybrid DFT [Pee15; Var10]. The latter achieves more accurate results concerning the band gap.

Peelaers *et al.* [Pee15] deduced that the fundamental band gap is indirect with a magnitude of 4.84 eV though the direct band gap is only 0.04 eV larger. The same result was obtained by Varley *et al.* [Var10] in addition to an analysis of the dipole matrix elements. As a result the authors state that the indirect transition is about an order of magnitude weaker than the direct transition, making β-Ga_2O_3 effectively a direct-gap material. Janowitz *et al.* [Jan11] published their findings from angle-resolved photoemission spectroscopy (ARPES) measurements and deduced that β-Ga_2O_3 has an indirect band gap with the value of 4.85±0.1 eV.

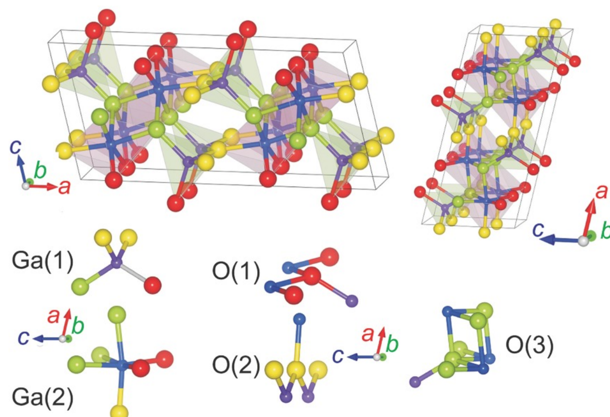

Fig. 3.2: Ga_2O_3 unit cell and inequivalent Ga/O atom positions [Wen17]. Copyright ©2017, John Wiley and Sons.

Besides the nature of the band gap, its size should make Ga_2O_3 an intrinsic insulator. However, if not grown stoichiometric a considerable n-type conductivity is observed. Its origin is either ascribed to oxygen vacancies [Ued97] or Si impurities [Ste16] in the host material. However, Varley and co-workers [Var10] calculated that oxygen vacancies act as deep donors with activation energies around 1 eV and, thus, are not expected to contribute to the conductivity. Apart from that, Ga_2O_3 can be either intentionally doped with Sn, Ge, Si, F, Cl [Ori00; Raf17; Var10] to achieve n-type conductivity or with Mg to compensate the free carriers in order to obtain insulating behavior [Gal10; Onu13]. Theoretical results by S. Lany [Lan18] conclude that Si is the only real shallow donor from the group 14 elements. Ge and Sn donor levels are situated close to the conduction band minimum in contrast to that of C which acts like a deep *DX*-like center. However, the possibility to successfully dope β-Ga_2O_3 p-type is still controversially discussed. Theoretical calculations from Varley *et al.* [Var12] conclude that it is impossible due to strong self-localization of holes. Kyrtsos and co-workers [Kyr18] reviewed cation dopants from groups 1, 2 and 12 by DFT and hybrid DFT calculations. As a result of their findings all dopants form deep acceptor levels, at least 1 eV deep, thus do not contribute to p-type conductivity at room temperature.

Table 3.1: Properties of β-Ga_2O_3

Property	Value	Reference
Crystal structure (Group symmetry)	Monoclinic (C2/m)	[Åhm96]
Lattice Parameters		
a	12.214 Å	[Åhm96]
b	3.037 Å	[Åhm96]
c	5.798 Å	[Åhm96]
β	103.832 °	[Åhm96]
Density	5.95 g/cm^3	
Melting Point	1795 °C, 1795 ± 15 °C	[Vil08], [Sch63]
Dielectric constant	9.9–10.2	[Pas95]
Band gap (direct)	4.9 ± 0.1 eV, 4.87 eV	[Jan11],[Var10]
Band gap (indirect)	4.85 ± 0.1 eV, 4.83 eV	[Jan11],[Var10]

CHAPTER 4

Deposition of thin films

A plethora of thin film growth techniques exist today suitable for depositing TCOs. Those can be divided into two main branches, namely chemical and physical methods. The most common chemical deposition techniques are atomic layer deposition (ALD), CVD and chemical solution deposition (CSD), whereas some of the physical methods are consolidated under the term physical vapor deposition (PVD) techniques. Characteristics of these are that all require vacuum conditions and physical effects are used for evaporation of the target material. More complex approaches are PLD, MBE, or the sputtering methods.

Both, the PLD and MBE, are more suitable for scientific research as upscaling for industrialization is not feasible on large substrates needed for photovoltaic thin-film applications. Furthermore, MBE needs base pressures in the ultra high vacuum range (10^{-10} mbar) resulting in extraordinary high efforts and costs to achieve and maintain an industrial production line.

Hence, for commercial utilization and upscaling the sputtering methods remain the most suitable techniques. During the last decades, conventional radio-frequency (rf) magnetron-assisted sputter deposition was thoroughly described and understood. Cathode sputtering methods all share on property – they need high energy ions in the plasma of the working gas in order to sputter off target ions of sufficient energy. A certain energy has to be passed by the ions to be mobile on the substrate or deposited film and to form a dense film of high quality. Another way of increasing the mobility of the adatoms provided by the target on the surface is heating of the substrate. Two obstacles occur. On the one hand, substrate heating may lead to interdiffusion in case of multilayer thin-films or damage of the material in case of temperature sensitive substrates e. g. polymer materials. On the other hand, transferring more energy to the target atom by the ions of the plasma is limited by the damage threshold of the target and its destruction.

A maximum power density of $300\,\mathrm{W\,cm^{-2}}$ on the metal target was published by Posadowski for DC magnetron sputtering [Pos95]. In comparison, a pulsed DC glow discharge yields a maximum target power density of about $900\,\mathrm{W\,cm^{-2}}$ [Gru91]. These limitations in power density can be overcome by an emerging new technique in DC sputtering. Here, an additional pulse sequence on-off is applied allowing one to increase the sputtering power during on-times to even higher values, e. g. $2.5\,\mathrm{kW\,cm^{-2}}$ [Čap13]. This method is referred to as high-power pulsed magnetron sputtering (HPPMS) [Kel09; Sar10]. Employing HPPMS in the growth of InGaN allows one to lower the deposition temperature by 200 °C while maintaining high crystal quality [Nak14; Sho14]. This reduction of substrate temperature is also desirable when conducting depositions on temperature sensitive substrates and in terms of costs. This makes the sputter deposition in pulsed mode a promising technique for achieving high kinetic energies of the adatoms from the target on the substrate at low substrate temperatures, and thus denser films of better quality.

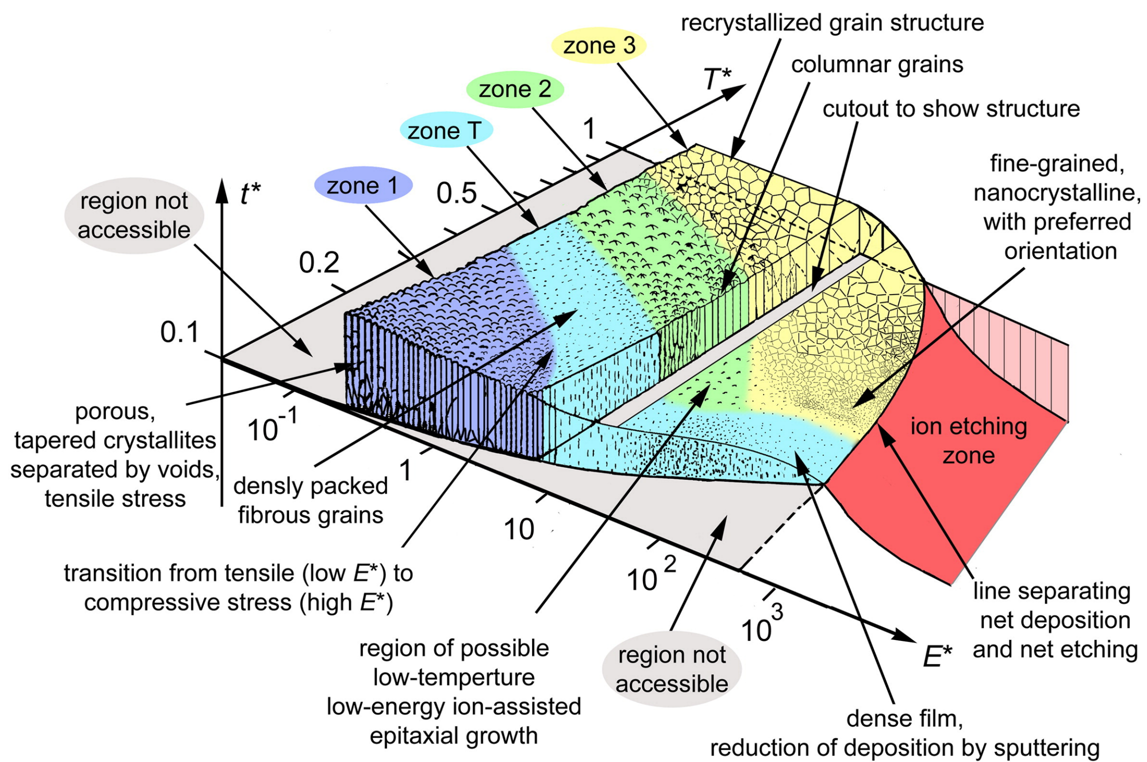

Figure 4.1: Structure zone diagram applicable to energetic depositions. Copied from A. Anders [And10]. Copyright ©2009 Elsevier B.V. Published by Elsevier B.V. All rights reserved.

The explanation for this behavior was first given by J. Thornton and D. Hoffman [Hof94; Tho89, and references therein]. It was further expanded to include high-power

impulse magnetron sputtering (HiPIMS), or also called HPPMS, and ion etching by A. Anders in 2010 [And10]. To have a more universal structure zone model the original process axes parameters chosen by Thornton and Hoffman were changed from substrate temperature relative to the melting point and argon pressure to a generalized temperature T^*, generalized energy E^* and layer thickness on the z-axis. The difference to the previously chosen parameters is that the expanded model also covers particle energies. In particular, the influence of the potential energy transfer between working gas ions and target atoms on the growth temperature, is included in T^* and the kinetic energy influence on the mobility of adatoms as well as induced heating is summarized in E^*. Figure 4.1 shows different growth zones and how they depend on the parameters mentioned, e. g. decreasing temperature can be compensated by increasing the energy in order to maintain the same growth zone. With this relationship the challenge of a limited heating power can be overcome by increasing the kinetic energy of the target atoms impinging on the substrate (E^*).

The same effect can be accomplished in the available setup at the Institute of Experimental Physics I by a combination of the conventional rf sputtering and the pulsed deposition. Here, a periodic superimposed rectangular voltage pulse repeated with the so called pulse repetition frequency (PRF), switches the rf signal periodically on and off. Voltage pulse duration with respect to cycle duration defines the pulse duty cycle (PDC). Varying the PDC the average power density per cycle can be kept constant (responsible for target damage) whilst achieving much higher power densities during on-times (determining the kinetic energy of the adatoms on the substrate). The characteristic quantities depend on each other. Exemplary, the minimum value of the PDC is dependent on the PRF and on the radio-frequency generator (RFG) used. This method is not straightforward and has not been reported in literature before. However, it offers manifold possibilities for improving thin-film growth. Some of the most striking results and investigations performed in the framework of this PhD project are described in the next chapter.

CHAPTER 5

Growth of β-Ga_2O_3 layers

Continuous-mode rf magnetron sputtering

Manifold factors can influence the quality of a deposited layer in a sputter deposition process, e. g. the gas composition, growth temperature, rf power or choice of substrate. These parameters not only influence the final layer quality but also correctly adjusted trigger counter measures avoiding preferential sputtering or limited heating capabilities of the setup. The former, preferential sputtering, is always present as soon as more than one element is provided by a PVD target [Kel78]. For example, in a sputter deposition from a ceramic binary target, like Ga_2O_3, preferential sputtering of the metallic species, i.e. excess of Ga, can be compensated by increasing the O_2:Ar ratio within the sputtering gas. Nevertheless, due to the polymorphism of Ga_2O_3, cf. Fig. 3.1, the growth temperature still plays an important role in achieving phase-pure material. In such a process, different thermal conductivities of the underlying substrates need to be taken into account. While for quartz glass thermal conductivity rises with increasing temperature, sapphire substrates exhibit a thermal conductivity maximum at about 50 K and a decrease at higher temperatures [Sal06]. The change of particle energy induced by rising sputtering powers can also influence the condensation of phase pure material positively. However, if the energy is too high, it may also foster re-evaporation of condensed particles or particle implantation into the deposited layer disturbing the crystal lattice. For the sake of completeness, an indirect influence of varying the rf power has to be considered, showing up in form of substrate heating. Even with the substrate heater switched off, substrate temperatures of 200 °C are not unusual due to the interaction with the plasma.
The impact on the layer quality of this complex system of interdependencies between the various parameters was investigated in this work. Different methods like XRD, optical transmission and reflectance spectroscopy measurements, SEM or XPS were used to characterize the deposited layers. A well-known correlation between increasing sputtering power or substrate temperature and layer quality was verified by XRD. However, the crystallinity did not improve significantly in the parameter space

accessible. Utilizing the results of the optical measurements it was possible to calculate the layer thicknesses of the layers by applying the dispersion relation of the refractive index determined by Rebien *et al.* [Reb02] to the interference oscillations visible in the reflection and transmission spectra. A linear increase in rf power resulted in a linear gain of layer thickness, but also triggered a slight crystal lattice deterioration. However, the difference in substrate temperature behavior of sapphire mentioned above was reflected by decreasing layer thicknesses when the maximum heating power was approached. For a validation of the calculated layer thicknesses, SEM measurements of the cleaved edge of some samples were performed and revealed discrepancies between calculation and measurement. Furthermore, the discrepancy can depend on the parameters varied. In particular, one direct correlation was affirmed by XPS measurements. The discrepancy between actual layer thickness determined from the cleaved edge and the calculated value based on the published refractive index dispersion was larger for non-stoichiometric Ga_2O_3 where the ratio of O:Ga deviated from 1.5. With variation of the Ar:O_2 ratio in the sputtering process the Ga_2O_3 stoichiometry can be adjusted. It was concluded, that the dispersion relation of the refractive index depends on the stoichiometry of the layer. The refractive index dispersion was derived for non-stoichiometric Ga_2O_3 and it was suggested that it may offer an easy approach to investigate Ga_2O_3 stoichiometry by an optical measurement.

In my work, the quality of the deposited layers was considerably improved, but unfortunately was still too low for utilization as a functional layer in devices. One way to improve the layer quality further is given by post-deposition temperature treatments. Another alternative is changing, or adapting, the approach used to deposit the layers to better fulfill the requirements needed. Presumably, one major cause for the insufficient layer quality is the low energy of particles condensing on the layer or substrate surface, increasing this energy should improve crystallization. Accordingly, either the substrate temperature has to be further increased or the arriving target atoms have to possess more kinetic energy to foster ideal condensation conditions. Due to plant-specifics the former is not possible and the latter, by increasing sputtering power, exhibits a high probability of target destruction due to too high continuous power application, e.g., due to arc events at the target.

Pulsed-mode rf magnetron sputtering

A promising way to prevent target destruction in the sputter deposition process from happening while still drastically increasing the energy of the particles arriving on substrate or layer surface is to utilize a pulsed-mode operation, known from pulsed DC sputtering. Doing so, missing heating capabilities can be counterbalanced by increased secondary particle energy to facilitate crystal growth along preferential

orientations. By utilizing a pulsed plasma mode and, therefore, non-continuous sputtering, the applied rf power to the ceramic targets was drastically increased, i.e. to values between 600 and 1000 W. The power densities achieved here, 13.2 to 21.9 $W\,cm^{-2}$, seem to be low compared to the values mentioned above for sputtering metal targets but are high compared to other ceramic materials like Al_2O_3 with up to 9.9 $W\,cm^{-2}$ [Gar16]. Similar to conventional rf sputtering the rise in applied rf power is supposed to increase the particle energy of primary and secondary species. Consequently, an increase of the evaporation rate results in thicker layers and, due to higher secondary particle energies, better crystal properties are achieved. However, it may also happen that the layer grows too fast for well-ordered adatom positioning and layer arrangement. In this case, the crystallinity will be lower than expected. This is anticipated at very high sputtering powers. Thus, the challenge remains to find the right power setting where optimum crystallinity is achieved. Additional parameters such as pulse repetition frequency and pulse duty cycle, have to be investigated in more detail as current literature is scarce. While the former parameter was kept constant at 1 kHz, the pulse duty cycle, describing the ratio of plasma on-time and period, was increased in steps of 10% up to 70% during a second growth series. With the pulsed rf sputtering mode an extra parameter, the plasma on-time, was introduced to account for the product of pulse duty cycle and total sputtering time. In this work, the plasma on-time was kept constant at 6 min. The variation of sputtering power and pulse duty cycle yielded two series, which were analyzed thoroughly by different methods in their as-deposited (AD) and rapid thermal annealed (RTA) states.
Analogous to conventional sputtering the linear variation of the rf power led to an increase of the layer thickness; only slight differences were identified between measurements of AD or RTA layers. Comparing the values of the optical band gap of conventional and pulsed-mode sputtered layers revealed a significant difference. The determined optical band gaps of the layers deposited by pulsed-mode approach the literature value of β-Ga_2O_3 from above and agree only for highest rf powers. In conventional rf magnetron sputtering this was the case for the lowest applied rf powers. This difference was tentatively assigned to two superimposed effects: First, to the relation between rf power and preferential sputtering effect, and second to a shift of the observed tendency to higher band gaps by pulsed-mode operation. The relationship between the process parameters of pulsed-mode and continuous-mode operation in a deposition processes is unknown. For example, the relationship between oxygen flux and connected primary particle energy has to be refined. Nevertheless, there is no clear explanation for the larger band gaps, though different, possibly superimposed, effects might be mentioned. The rf power in pulsed-mode is three to five times higher than the maximum power used in the conventional sputtering mode. As a consequence, the secondary particle energies are significantly increased permitting the direct formation of bonds on nucleation. Possibly, crystallites may

contain a sesquioxide or spinel-type layer structure and may be strained as well, i.e. no clear statement about band gaps can be made. The optical band gap of an amorphous phase would be expected at about 4 eV and is thus no valid explanation [Zha18]. Furthermore, the negatively charged oxygen species are also influenced by the higher applied power enabling them to penetrate deep into the Ga_2O_3 layer. Kumar *et al.* [Kum13] ascribed slightly higher band gaps to excess oxygen within the layer. After rapid thermal annealing of the deposited layers the optical band gaps increased and seemed to saturate at about 5.0 eV. This enhancement might be ascribed to Al diffusion from the substrate into the deposited layer creating meta-stable phases like $(Ga,Al)O_3$. Furthermore, due to the chemical similarity, it is possible to substitute Ga and Al in their respective lattices easily. A more detailed discussion of the interdiffusion phenomena can be found in Appendix B.

In spite of the good agreement of the determined layer thicknesses and optical band gaps between Ga_2O_3 samples grown in the two modes, the opposite is true for the results obtained from XRD measurements. The determined state of crystallinity is predominantly amorphous although some broad peaks were identified as the (400), (-313) and (-603) peak series reflections of β-Ga_2O_3 which may be superimposed by (300) and (018) peaks of α-Ga_2O_3, the (111) peak series of γ-Ga_2O_3 or the meta-stable $(Ga,Al)O_3$. The results illustrate well that a certain particle energy has to be reached to form the necessary bonds or to disturb the substrate surface sufficiently to generate the meta-stable materials. After rapid thermal annealing, only those peaks in the XRD traces remain which are related to the β-phase as the other phases already vanish at temperatures way below the treatment temperature. With increasing sputtering power the positions of the (-201) peak series shift towards the value of bulk β-Ga_2O_3 material while maintaining the correct intensity ratio [Nak12; Ori02; Osh07].

Considerable improvements in layer quality were observed, which can be mainly attributed to the increase of applied rf power. As the next step, the pulse duty cycle was varied and thus the power load transferred to the target. Accordingly, the sputter ion energy increases with increasing duty cycle as the successive acceleration time is enlarged and the time without an electric field present is decreased. To achieve comparability with the preceding series the parameter "plasma on-time" was maintained constant, i.e. the total sputtering time was decreased with increasing duty cycle value.

In contrast to the straightforward relationship between rf sputtering power and layer thickness, the situation is much more complicated for that between pulse duty cycle and layer thickness. The on-time of the plasma, i.e. the acceleration time of ionized atoms, is prolonged when the PDC value is increased. This not only influences the particles energy dispersion but also the distribution of species and the interaction cross sections of primary ions with the target material, and consequently, the properties

of secondary ions as well. A first implication was identified as a non-linear layer thickness evolution tentatively assigned to the changed energy distribution. Re-evaporation of condensed particles or increased presence of negatively charged oxygen ions etching the deposited layer are the most likely consequences. Another possible result of the increasing PDC, underlining the necessity to optimize the parameter space for each PDC, is given by the strongly decreasing optical band gap. Values below the literature value correspond to high PDC values and might be explained by an increased defect density caused by insufficient time for the arrangement of the target atoms arriving on the surface of substrate or deposited layer. Post-deposition temperature treatments nearly have no influence besides the Al diffusion described above for thin layers, i.e. low PDC values. Another implication is the disappearance of reflections of low XRD intensity, observed already previously and tentatively assigned to γ-Ga_2O_3 or meta-stable $(Al,Ga)O_3$, although differences exist compared to previous results. A set of reflections belonging to the $\{-h01\}$ family of planes is found in RTA layers and is more pronounced compared to as-deposited layers suggesting the supposition that higher formation energies are required which are only available at elevated duty cycle values.

One distinct parameter set, 800 W and 30% PDC, was chosen for in-depth analysis of the crystallinity and existence of assumed interface related phases. All applied methods, SEM, AFM and Raman measurements confirmed an increase in crystallinity after annealing while especially Raman spectroscopy is known to very sensitively differentiate between the different material phases present in case of the Ga_2O_3 system. However, to investigate the real physical interface region TEM measurements had to be performed to utilize the unmatched atomic resolution of this technique. Polycrystalline material was confirmed by measured SAED patterns underlining the previous hypothesis of crystalline domains in an amorphous matrix. Even more details were obtained, e.g. differentiation between different domain orientations, by cross-sectional TEM. A continuation of the substrate structure for some nm with higher signal strength, i.e. Al atoms were replaced by Ga atoms, was observed. Furthermore, the interface region was not sharp indicating interdiffusion most likely caused by impingement of negatively charged oxygen. The gathered results underline, that the investigated pseudomorphous grown interface layer can be assigned to γ-Ga_2O_3. Nevertheless, it should be noted that literature states α-Ga_2O_3 can also be observed at the sapphire interface. Although this was not the case in the experiments performed here, presence of this additional polymorph cannot be completely excluded.

CHAPTER 6

Summary and Outlook

In the framework of this dissertation, layers of the transparent conducting oxide Ga_2O_3 were deposited by rf sputter technology in continuous-mode and pulsed-mode operation. Afterwards, the grown thin films were thoroughly analyzed by various methods in their as-deposited state as well as after post-deposition thermal treatment. The intended application for the grown layers was the utilization as window layer in Cu_2O-based thin film solar cells.

Whilst the conventional sputtering was not suitable to achieve highly crystalline material still valuable insights were gained. Amongst them was the possibility to identify non-stoichiometry of material systems by determining the wavelength-dependent refractive index and comparing it to the literature value of the respective bulk material. Furthermore, both possible ways taken to improve layer quality, namely increasing rf power and/or heating power, indeed enhanced the available kinetic energy of secondary particles, however, not sufficiently to grow high grade material yet. Moreover, post-deposition temperature treatments showed the capability for slight improvements, but triggered stronger interdiffusion between deposited layer and underlying substrate.

The major driver for the development of this novel pulsed-mode methodology of sputter deposition was to resolve plant-specific limitations which could not be overcome without risking target damage or machine failure. Due to these constraints, technically speaking the limited heating capabilities as well as the applicable power density to the target, the effort to further improve layer quality was at its limit. Now, the correlation of the conventional sputtering parameters, e. g., gas composition or rf power, with the additional pulse-mode specific ones, e. g., pulse duty cycle or pulse repetition frequency, opened a novel field of research which will have to be explored in-depth in the future. This exploration was started with the systematic variation of the PDC value at a given set of PRF and rf power values. Unambiguously, the influence on plasma kinetics, e.g. the ion species and energies, was witnessed as thinner layers exhibited much larger optical band gaps compared to conventionally deposited layers with equal thickness. Besides, the layer thickness evolution also showed non-linear

behavior which was explained preliminarily by an increased presence of negatively charged oxygen ions and modified plasma properties. However, more experiments need to be performed to confirm this assumption. X-ray diffraction measurements underlined the difference between the novel layers obtained in pulsed-mode over conventionally sputtered layers. Peaks were identified in the XRD traces which are either assignable to the metastable γ-phase of the gallium sesquioxide or to an alloy of Ga_2O_3 and Al_2O_3, i.e. the *c*-plane sapphire substrate. This assumption was further verified by repetition of the XRD measurements after thermal treatment at 1000 °C yielding a disappearance of some peaks which can be explained by transformation of the layer into the thermodynamically most stable form of Ga_2O_3, the β-phase. A detailed examination of the interface region between the two adjacent materials was made possible by TEM measurements. Continuation of the crystal structure of the sapphire substrate was observed in the Ga_2O_3 layer though with brighter signal intensity, explainable by Al replacement by Ga. These findings lead to the tentative assignment of the pseudomorphous grown region to γ-Ga_2O_3.
Accordingly, pulsed rf sputtering succeeded in improving the layer quality slightly but with the drawback of mixed phase creation. However, reconsidering the intended application another hindrance arises due to the limited temperature stability of the absorber material Cu_2O. Hence, the elevated temperatures needed for the deposition of crystalline Ga_2O_3 will without doubt cause serious degradation or even deterioration of the absorber layer. This may be avoided modifying the cell design – i.e. to deposit the temperature sensitive layer on top of the window layer. Given the success of this design modification another obstacle would prohibit a commercialization as costly substrates are needed for deposition at high temperatures. The choice of substrate either limits the size of the final solar cell or raises the costs of fabrication. Nevertheless, with ongoing exploration of the complex parameter space it is very likely that a set of parameters exists and will be found yielding high-quality Ga_2O_3 layers. Above all, the results shown here for this new methodology will without doubt help to overcome similar problems in other material combinations with less thermal energy requirements.

During the final stage of this dissertation parallel investigations into the deposition of Ga_2O_3 by ion-beam sputtering were performed. This methodology provides very precise control of the primary ion energies extracted from the ignited plasma by the extraction grid. The optimization of the parameters growth temperature and oxygen partial pressure yielded in dependence on the sapphire substrate used out-of-plane orientation phase-pure Ga_2O_3 polymorphs of exceptional, almost epitaxial, quality [Bec20]. Consequently, heterostructures made of Cu_2O and Ga_2O_3, either α- or β-phase, were grown and examined via X-ray photoelectron spectroscopy (XPS) [Ben].

CHAPTER 7

Publication Manuscripts and Contributions

7.1 Optimizing the Stoichiometry of Ga_2O_3 Grown by RF-Magnetron Sputter Deposition by Correlating Optical Properties and Growth Parameters

Published in Phys. Status Solidi A **2019**, *216*, 1900385 [Sch19]

Clarification of my own contribution to the publication:

I deposited the majority of the analyzed samples and performed the optical transmittance and relative specular reflectance, X-ray diffraction and scanning electron microscopy measurements. Interpreting this data, the correlation between optical properties and growth parameters was developed and discussed with my co-authors. Finally, I wrote the manuscript.

physica status solidi pss a
www.pss-a.com

Optimizing the Stoichiometry of Ga_2O_3 Grown by RF-Magnetron Sputter Deposition by Correlating Optical Properties and Growth Parameters

Philipp Schurig, Marcel Couturier, Martin Becker, Angelika Polity, and Peter Jens Klar*

β-Ga_2O_3 thin films are deposited by radiofrequency (RF)-magnetron sputtering on quartz and c-sapphire substrates using a ceramic stoichiometric Ga_2O_3 target and a constant flux of argon process gas. Oxygen flux, heater power, and sputtering power are varied in the synthesis of the layers. The resulting Ga_2O_3 layers are analyzed in terms of their structural and optical properties. Based on this analysis, the process parameters leading to the formation of an optimized β-Ga_2O_3 layer are identified. The main challenge in obtaining the stoichiometric β-Ga_2O_3 thin films by sputter deposition is to overcome the influence of a strong preferential sputtering of Ga from the ceramic target. This can be achieved by adding a suitable fraction of oxygen to the argon process gas used in the deposition process. Furthermore, it is demonstrated that the refractive index dispersion of β-Ga_2O_3 depends strongly on its composition. Thus, a combined analysis of refractive index dispersion and optical bandgap position may serve as a valuable preliminary probe of the thin film's composition.

1. Introduction

The generation of energy from renewable energy sources, for example, conversion of solar energy into electric energy by solar cells, is still a major research area. The driving force is to reduce fossil fuel consumption and, thus, to stop, or at least postpone, global warming. It requires a mass production of solar cells as well as an efficient use of all available areas for installing such devices for photovoltaics to yield a viable contribution to the world's energy supply.

Transparent conducting oxides (TCOs), which exhibit almost metal-like conductivities in addition to a large bandgap (>3 eV), play an important role in thin-film photovoltaics concepts.[1,2] These serve as transparent top contacts forming the p–n junction to a smaller bandgap absorber in thin-film photovoltaics. The quest for absorber materials based on abundant chemical elements is on and necessary to realize corresponding thin-film solar cells on mass production levels. Thin-film photovoltaics on glass substrates and based on abundant semiconductor materials may offer a cheap alternative to the established technologies. Another interesting possibility for further integration of photovoltaics into modern life is to develop transparent solar cells, for example, windows that may also act as solar cells and contribute to the energy supply.[3] As this approach requires materials that are conductive and transparent at the same time, TCOs are likely candidate materials for this purpose.[4]

The p–n junction is the central building block of a thin-film photovoltaic cell as it generates the built-in electric field to separate charge carriers generated by absorption of light. Recently, cuprous oxide, Cu_2O, with its bandgap of 2.1 eV is discussed as a suitable and promising p-type absorber material[5–7] based on abundant chemical elements. To tap the full potential of Cu_2O as absorber material in thin-film solar cells, it needs to be combined with a suitable n-type semiconductor. "Suitable" means that the band alignment at the junction does not exhibit high-band offsets, in particular, in the conduction band. β-Ga_2O_3 is discussed as a promising candidate, because of its low-electron affinity close to that of Cu_2O, it exhibits a very low discontinuity in the conduction band.[8,9] Furthermore, Ga_2O_3 has a large bandgap close to 5 eV[10–12] and thus forms an ideal top contact on Cu_2O, when doped n-type. In case of a transparent solar cell, both constituents on either side of the junction, p- and n-type semiconductors, have to be transparent. Nowadays n-type semiconducting transparent materials are state of the art, but suitable p-type conductors still need to be identified.

For the reasons outlined earlier, there is a considerable interest in Ga_2O_3 in the context of photovoltaics. The material and its processing offer various degrees of freedom for optimizing its structure for a specific application. Five different crystalline phases of Ga_2O_3, denoted as α, β, γ, δ, and ε phase, are known to date.[13] The β-phase has the highest thermal and chemical stability among those five phases.[14,15] Moreover, the crystal structure, conductivity, as well as optical bandgap of Ga_2O_3 can be influenced by the changes in process parameters or by post-thermal treatment.[16,17] Thus, a controlled manufacturing process for β-Ga_2O_3 is a hot topic of applied research in photovoltaics.

Ga_2O_3 thin films may be prepared by various methods, including molecular beam epitaxy (MBE),[18–20] metal-organic chemical

P. Schurig, M. Couturier, Dr. M. Becker, Dr. A. Polity, Prof. P. J. Klar
Institute for Experimental Physics I and Center for Materials Research (LaMa)
Justus Liebig University Giessen
Giessen, Germany
E-mail: martin.becker@exp1.physik.uni-giessen.de

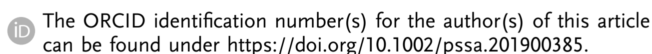
The ORCID identification number(s) for the author(s) of this article can be found under https://doi.org/10.1002/pssa.201900385.

DOI: 10.1002/pssa.201900385

© 2019 WILEY-VCH Verlag GmbH & Co. KGaA, Weinheim

vapor deposition (MOCVD),[21] pulsed laser deposition (PLD),[11,22] sol gel,[23,24] chemical vapor deposition (CVD),[25–27] and sputtering techniques.[15,17,28–31] The reported growth rates of stoichiometric Ga_2O_3 thin films are comparatively low. Typical growth rates of Ga_2O_3 thin films grown by MBE and PLD are 0.04[20] to 0.09[32] and 0.22 $\mu m\,h^{-1}$,[33] respectively. An increase in the growth rate of Ga_2O_3 films is desirable in terms of mass production of devices and can be obtained by means of RF-magnetron sputtering with deposition rates >1 $\mu m\,h^{-1}$.[17]

In this study, we discuss the deposition of Ga_2O_3 thin films on quartz and c-sapphire substrates using RF-magnetron sputtering. Heating power, sputtering power, as well as oxygen flow were varied. Subsequently, β-Ga_2O_3 films were investigated to optimize the deposition conditions according to β-Ga_2O_3 growth. Refractive index dispersion was determined for stoichiometric and nonstoichiometric Ga_2O_3 thin films and compared with the limited data in literature available on sputtered Ga_2O_3 samples.[30,34]

2. Experimental Section

We deposited Ga_2O_3 thin films on quartz and c-sapphire substrates by RF-magnetron sputtering. In sputtering, ions of the process gas—in our case, a gas mixture of inert Ar and reactive O_2—impinge onto a target, here a Ga_2O_3 ceramic target and sputter off target atoms. The target atoms react with the reactive species of the process gas and form a film, here a Ga_2O_3 film, on the substrate, which is located opposite the target surface. Prior to each deposition, the substrates were cleaned with acetone and methanol in an ultrasonic bath for 3–5 min and then dried with nitrogen. Subsequently, the substrates were mounted in a cylindrical sputter chamber (base pressure of 5×10^{-7} mbar) at a distance of 5 cm below the target to assure lateral homogeneity.

Here, we discuss three series of samples. Throughout each series a specific process parameter was varied systematically, while all the other process parameters were kept constant (**Table 1**). The variables chosen were Ar:O_2 ratio in series I, substrate temperature in series II, and RF power in series III. In case of series II, the substrate temperature was varied by adjusting the heating power of the temperature controller (model Eurotherm 2408). The interval of 465–1440 W nonlinearly translates to a temperature window between 385 and 581 °C on the substrate surface in vacuum, without a plasma being present. A distinct characteristic is given by an interplay of the substrate's thermal conductivity and its effectiveness in emitting energy as thermal radiation. The actual growth temperatures (surface temperatures) may be considerably higher depending on the RF power coupled into the plasma of the process gas and the distinct thermal directional characteristic. This enhancement of the surface temperature by the presence of the plasma is estimated to be up to 200 °C at the highest RF power used. The RF power was generated by a Dressler CESAR 1312 system equipped with a Dressler VM 1500 AW matching network and was varied between 50 and 200 W. It should be noted that the surface temperatures in vacuum for quartz substrates are 50 °C lower than those for sapphire substrates at the highest heating power. This finding is related to the lower thermal conductivity of quartz in the temperature range relevant in the growth process.

The films were analyzed by X-ray diffraction (XRD, Siemens D 5000) in a Θ–2Θ geometry. Optical transmittance at normal incidence ($\beta = 0°$) and relative specular reflectance close to normal incidence ($\beta = 6°$) were recorded using a PerkinElmer Lambda 900 spectrometer. The influence of the substrate was eliminated by measuring the substrate baseline prior to thin film deposition. Most thin films discussed possess layer a thicknesses >1 μm.

Table 1. Parameters used in sputter processes for depositing sample series I–III.

Series	Ar flux [sccm]	O_2 flux [sccm]	RF power [W]	Heating power [W]
I	45	8–15	200	465
II	45	12.5	200	465–1440
III	45	12.5	50–200	1135

3. Results and Discussion

Figure 1a–c illustrates the X-ray diffractograms of Ga_2O_3 layers of series I, II, and III grown on quartz substrates. The findings are very similar in case of the series on sapphire substrates, but the corresponding XRD traces are dominated by strong and sharp sapphire reflections and are, thus, not shown here.

In series I, no significant change arises as a function of oxygen flux, that is, variation of the Ar:O_2 fraction of the process gas used in deposition (Figure 1a). However, this is somewhat expected because when using a stoichiometric target, a slight variation of the O:Ga ratio in gallium sesquioxide seems more likely than the formation of suboxide phases. Heating power was at the lowest setting of 465 W, and RF power coupled into the process plasma was 200 W. All diffractograms reveal rather broad signals at about 30°, 35°, 45°, 57°, and 64°. Characteristic reflections of β-Ga_2O_3 are given on top of the figure and are indicated by green vertical lines. A comparison with reflections reveals the polycrystalline character of deposited layers. This is in contrast to the findings of Kang, who found Bragg reflections only for the {–201} β-Ga_2O_3 family of planes on c-sapphire substrates and concluded that this is the preferred orientation in surface-normal direction.[29] It should be noted that in the findings of Kang thin films were deposited at 645 °C, whereas our samples (Figure 1a) were grown at temperatures <600 °C. Thus, we believe a minimum growth temperature, among others, is a mandatory condition for obtaining β-Ga_2O_3 thin films on c-sapphire substrates with a preferential orientation. A similar behavior was found for β-Ga_2O_3 sputter grown on silicon substrates where the as-deposited samples exhibited an amorphous XRD pattern, and annealing temperatures ≥900 °C were necessary for obtaining polycrystalline material.[15,17]

Figure 1b shows the results of series II where heater power and, thus, surface temperatures of the substrate were varied. Ar and O_2 flux were set to 45 and 12.5 sccm, respectively, and the RF power coupled into the process plasma was again 200 W. Crystallinity improved on increasing the heater power from 465 to 900 W, indicated by the sharpening of the reflections. However, no further improvement was observable >900 W. A heating power of 1135 W; and Ar and O_2 flux set to 45 and

© 2019 WILEY-VCH Verlag GmbH & Co. KGaA, Weinheim

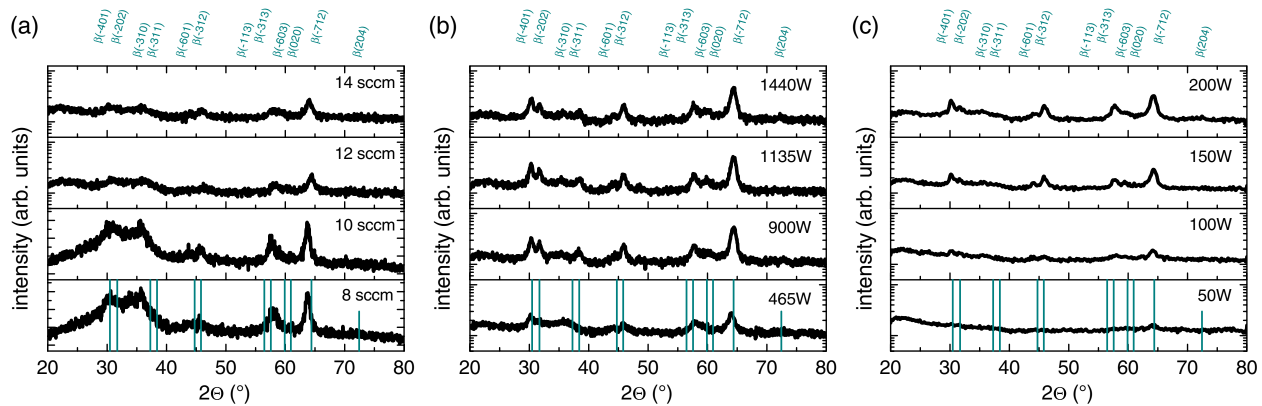

Figure 1. a) X-ray diffractograms of Ga_2O_3 grown on quartz. Changing the Ar:O_2ratio in sputter atmosphere does not alter crystallinity significantly, whereas several orientations are observed. This polycrystallinity is also verified for b) series II (substrate temperature) and c) series III (RF power).

12.5 sccm, respectively, were kept constant in series III, whereas the RF power and consequently also the kinetic energy of the ion species of the process gas were varied between 50 and 200 W. The diffractograms of the corresponding samples (Figure 1c) show first a slight increase in intensity and number of peaks toward a higher RF power up to 150 W. A further increase in the RF power to 200 W resulted in no additional improvement of crystallinity. However, increasing the RF power is accompanied with a significant gain in the growth rate.[35,36] Thus, we believe that increasing the layer thickness by increasing the RF power while maintaining the deposition temperature counteracts a possible improvement in crystallinity due to more disordered growth.

Figure 2a depicts the optical transmittance spectra of Ga_2O_3 layers of series I on quartz and c-sapphire substrates in the wavelength range of 260–400 nm. Above a wavelength of 360 nm, transmittance of all thin films was about 80–100%, presenting interference oscillations between light transmitted directly and light reflected at the back and front interfaces prior to being transmitted. Using the dispersion relation of refractive index given by Rebien et al. for RF-magnetron-sputtered samples,[34] whose composition was monitored by Rutherford backscattering, layer thickness d may be derived from the interference pattern. The corresponding values are shown in Figure 2c together with thickness values deduced from scanning electron microscopy (SEM) images of the edge of cleaved samples. The comparison indicates that—as expected from the variation of growth parameters, in particular, oxygen flux—the assumption of a stoichiometric sample is not valid in all cases. Indeed, preliminary measurements by X-ray photoelectron spectroscopy (XPS) show that samples of the oxygen flux series deviated from O:Ga = 1.5. We evaluated core-level O 1s, Ga 2p, and Ga 3d and found Ga concentrations up to 44% for low oxygen flux, whereas values close to 40% were found for highest oxygen fluxes used in series I.

Therefore, we decided to use the values of layer thickness obtained by SEM analysis of cleaved edges in conjunction with interference oscillations observed to derive refractive index dispersions of selected Ga_2O_3 samples grown. This allowed us to assess the magnitude of refractive index variation introduced by nonstoichiometry. Results for selected samples of all three series are shown in **Figure 3**. The corresponding growth parameters are given in the legend of the figure; the error bars represent uncertainties in layer thicknesses and the extremas' wavelengths in optical transmittance spectra. For clarity, only one error bar is shown per sample. The curvature of extracted

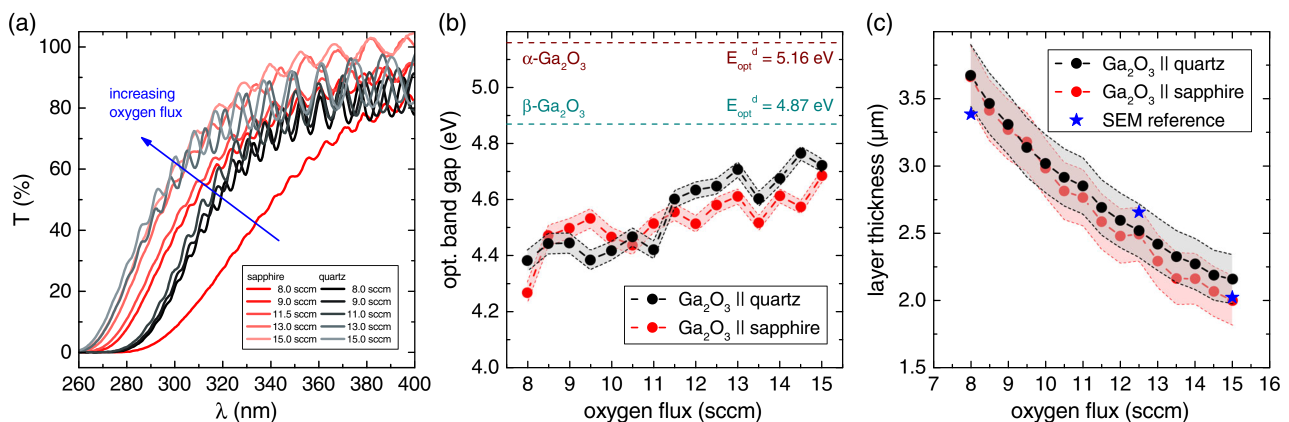

Figure 2. a) Representative optical transmittance spectra of Ga_2O_3 layers, deposited at different oxygen fluxes. Qualitatively, the dependence of b) optical bandgap and c) layer thickness is the same for Ga_2O_3 thin films deposited on quartz and c-plane sapphire, respectively. Asterisks in (c) denote the thicknesses determined by SEM analysis. Error margins given in (b) and (c) arise due to error in the refractive index used.[34]

© 2019 WILEY-VCH Verlag GmbH & Co. KGaA, Weinheim

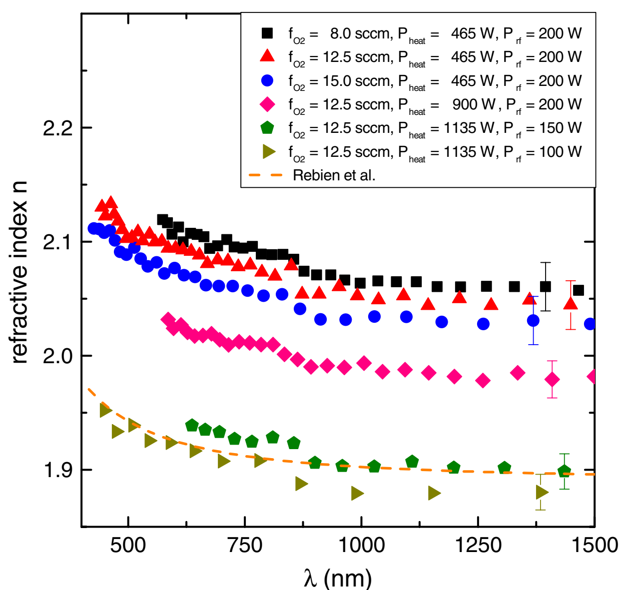

Figure 3. Refractive index dispersion of selected samples highlighting that nonstoichiometry triggers defective evaluation of thickness and optical bandgaps.

dispersion relations is comparable with that of dispersion relation derived by Rebien et al.[34] independent of composition. However, the absolute values of nonstoichiometric samples are considerably higher. This can be best seen in the long-wavelength regime where stoichiometric, crystalline β-Ga_2O_3 possesses a refractive index of about 1.9 in accordance with previously reported results,[30,34] and nonstoichiometric materials exhibit values almost up to 2.1. The analysis of the growth parameters yields that only the refractive index dispersion of samples prepared at a high heater power (i.e., high surface temperatures) and rather low RF power (i.e., low kinetic energy of ionic species of the plasma) match the dashed line representing the refractive index dispersion of stoichiometric β-Ga_2O_3. The error margins to the data points in **Figure** 2 and **4** represents the uncertainty due to an unknown degree of nonstoichiometry of the samples and corresponding uncertainties in the layer thicknesses. This uncertainty will not alter the trends and interpretations given in what follows. Furthermore, these findings will be important for future investigations of nonstoichiometric β-Ga_2O_3 or even Ga_2O_3-based alloys.

In the spectral range >400 nm, reflectance and transmission approximately add up to 100%, whereas <360 nm, measured transmittance drops due to absorption in the thin β-Ga_2O_3 films. At wavelengths λ where absorption dominates, the absorption coefficient α may be extracted using:

$$T(\lambda) = [1 - R(\lambda)] \cdot \exp(-\alpha(\lambda)d) \quad (1)$$

where α denotes the absorption coefficient, d the layer thickness, T the transmittance, and R the reflectance. The optical bandgap of Ga_2O_3 film can be estimated using Tauc's approach,[37] assuming a direct transition at the bandgap. Plotting α^2 versus $\hbar\omega$; and extrapolating the linear part of the curve to the abscissa yields the energy of the optical bandgap of the material studied, independent of its layer thickness.

For the samples of series I, on quartz as well as on sapphire, a shift in this onset of optical absorption toward lower wavelengths was found with increasing oxygen flux (Figure 2a). The optical bandgap of β-Ga_2O_3 layers increases with increasing oxygen flux (Figure 2b) and approaches the value reported for the bandgap of stoichiometric β-Ga_2O_3 of 4.87 eV from below. In agreement with the refractive index analysis, this behavior indicates that these samples are not stoichiometric and probably still oxygen-deficient.[14] The bandgap increases as the density of defects induced by oxygen deficiency is reduced with increasing oxygen flux. As the target consists of stoichiometric Ga_2O_3 and additional oxygen was used in the gas mixture, it may be anticipated, at first sight, that excess oxygen is present in the plasma and deposited layer. However, this consideration is in contrast with the optical data. Therefore, we believe that strong preferential sputtering occurs on the target, that is, gallium exhibits a much higher sputter yield than oxygen from Ga_2O_3 surfaces. Furthermore, in the same series of samples, we found that the growth rate was reduced with increasing oxygen flux as reflected by the layer thicknesses plotted versus oxygen flow in Figure 2c. The reason is that, as described earlier, the density

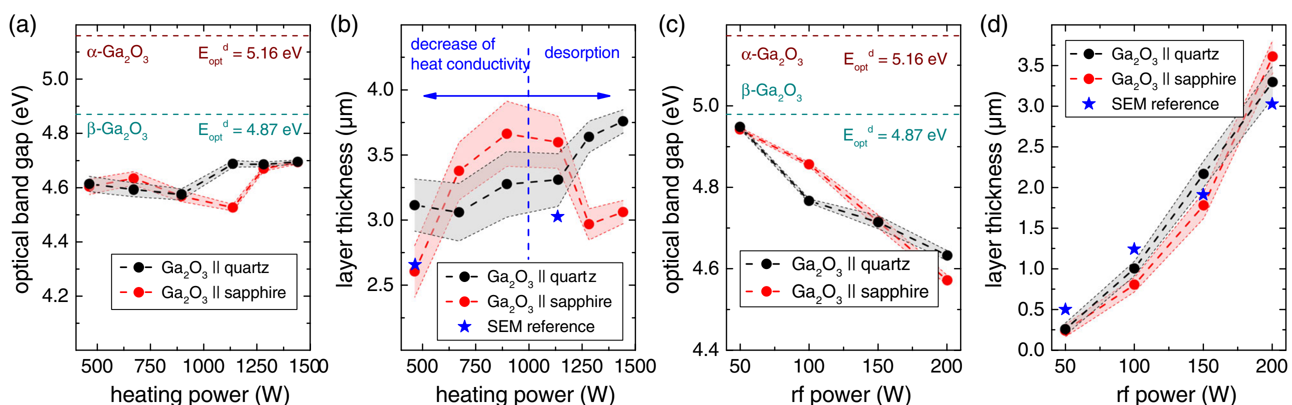

Figure 4. a,c) Optical bandgaps and b,d) layer thicknesses as a function of a,b) heater power applied during growth as well as c,d) RF power applied during growth. Asterisks in (b) and (d) denote the thicknesses determined by SEM analysis. Error margins given in (a–d) arise due to error in the refractive index used.[34]

© 2019 WILEY-VCH Verlag GmbH & Co. KGaA, Weinheim

of the process gas increased when the oxygen flow increased. As a consequence, the mean free path of the species in the plasma reduced and the rate of collisions of ions (which possess sufficient kinetic energy to sputter atoms off the target) with the target also reduced.[38] Moreover, the likelihood of the formation of negatively charged oxygen species in the plasma increased. Negatively charged ions accelerated toward the sample holder, which act as the anode. These oxygen species may etch the thin-film surface, further reducing the growth rate.[39]

Series II was deposited at different heating powers (Table 1) to see its impact on the thin-film growth. Figure 4b clearly reveals that the amount of heating power also affects the growth rate in addition to the degree of crystallinity. Furthermore, the trends observed for layers on quartz glass and sapphire substrates differ. The growth rate of the former increased steadily, whereas that of the latter exhibited a maximum in the intermediate heater power range. This behavior can be understood as follows. The diffusion rate of gallium and oxygen atoms on the substrate surface increased with increasing substrate temperature. It is the temperature that determines decisively how efficiently the atoms can arrange themselves on the surface. In general, a higher mobility of the species on the surface enables comparatively faster layer growth and higher crystallinity. However, the temperature can also be too high in the sense that the thermal energy is large enough to enable desorption of atomic species from the surface. Here the properties of the substrate come into play as the energy transfer from the heater arrangement to the substrate surface is determined, among others, by the substrate's thermal conductivity. The results in Figure 4b reveal clearly this influence on the substrate as quartz glass possesses lower thermal conductivity compared with sapphire.[40] The surface temperature of sapphire is about 50 °C higher than that of quartz glass at high heater powers. Note that this temperature difference was measured for substrates without plasma impact. Thus, the actual temperature difference might be even higher. In any case, the temperature corresponding to the onset of atomic desorption will be reached at a lower heater power in growth on sapphire surfaces, already at about 1000 W, than in growth on quartz glass, where it probably lies outside the accessible heater power range of the sputter system.

Figure 4a shows the behavior of optical bandgaps of Ga_2O_3 layers grown on the two types of substrates depending on substrate temperature. The bandgaps were again determined following Tauc's approach.[37] The observed trends were very similar, and even at the highest temperatures (heating powers), the value of 4.87 eV reported for the optical gap of stoichiometric bulk β-Ga_2O_3 could not be reached. However, the bandgap values were higher than those found for series I, somewhat indicating that growth at higher temperatures yielded a Ga_2O_3 material of better crystallinity, but probably not stoichiometric yet. For example, Sampath Kumar et al. showed that increasing the substrate temperature led to a reduction of the O:Ga ratio in their deposited Ga_2O_3 layers.[14] At room temperature, they observed an O:Ga ratio of 1.6, whereas at a process temperature of 600 °C, a stoichiometric ratio of about 1.5 was evaluated. Already at 300 °C, a clear trend toward an O:Ga ratio of 1.5 was shown.[14] Ramana et al. observed the same trend in their XPS analysis.[30] Thus, in any case, heating power plays an important role; however, an interplay of various factors such as crystal quality, defect structure, surface morphology, grain size, and composition might also affect the optical properties, rendering exact one-to-one transfer of conclusions difficult.

The results of Ga_2O_3 samples of series III grown at a high substrate temperature with different RF powers coupled to the plasma of the process gas are shown in Figure 4c,d. Clear trends were observed, which were similar for layers on both types of substrates. First, it should be noted (Figure 4c) that the samples of series III grown at the lowest RF power exhibited optical bandgaps closest to the theoretical value of stoichiometric β-Ga_2O_3. With increasing RF power, however, the optical bandgap values of Ga_2O_3 significantly decreased in a linear fashion. The growth rate (Figure 4d) showed the opposite trend and increased linearly with increasing RF power coupled into the plasma of the process gas. The results can be explained as follows. The lower the RF power coupled into the plasma, the less the kinetic energy of the process gas ions impinging on the target. The discussion of series I already showed that preferential sputtering is a major issue when using a Ga_2O_3 ceramic target in the growth process as the sputter yields of Ga and O were very different for this material. At the lowest RF power, the effect of preferential sputtering can be compensated by the excess oxygen in the process gas. Thus, the particle flux toward the substrate corresponds to the right stoichiometry. Furthermore, due to the low sputter rates at 50 W RF power, the atoms deposited on the substrate had more time to reach their positions and to form a film of better crystalline quality. We believe that weak X-ray diffractograms in Figure 1c obtained for the layers of series III grown at low RF power were rather due to small thicknesses of those films than due to lower crystalline quality, although a contribution of enhanced amorphization cannot be ruled out entirely.

4. Conclusions

Ga_2O_3 thin films were deposited by RF-magnetron sputtering from a ceramic Ga_2O_3 target onto quartz and c-sapphire substrates. Oxygen flux, heating power, and RF power coupled into the plasma of the process gas were varied systematically. Stoichiometric β-Ga_2O_3 polycrystalline thin films were obtained at moderate growth temperatures of about 600 °C, when a low RF power was used and the process gas contained excess oxygen. Excess oxygen is required to compensate the excess Ga in the particle flux toward the substrate arising from a strong preferential sputtering of Ga species from the target. The growth rate found for the best β-Ga_2O_3 thin-film material was rather low; however, the layer thickness determined still translates to a growth rate of 0.25 $\mu m\,h^{-1}$, a value comparable to the largest rates given in literature for other growth methods. Moreover, our results suggest that a low growth rate is not an intrinsic problem and may even be enhanced by coupling higher RF power into the plasma and simultaneously increasing the fraction of oxygen in the process gas. Refractive index dispersions and optical bandgaps extracted from UV/Vis optical transmittance and reflection spectra were successfully used to identify stoichiometric β-Ga_2O_3. In particular, we demonstrated that the refractive index dispersion of nonstoichiometric β-Ga_2O_3 strongly deviates from that of a stoichiometric material, an aspect that may play a role in optimizing the antireflection behavior of Ga_2O_3 transparent contacts on thin-film solar cells.

© 2019 WILEY-VCH Verlag GmbH & Co. KGaA, Weinheim

Acknowledgements

Financial support was provided by the DFG via the RTG (Research Training Group) 2204, "Substitute Materials for Sustainable Energy Technologies."

Conflict of Interest

The authors declare no conflict of interest.

Keywords

gallium oxide, refractive indexes, RF-magnetron sputter deposition, thin films

Received: May 9, 2019
Revised: July 31, 2019
Published online: August 25, 2019

[1] M. Grundmann, H. Frenzel, A. Lajn, M. Lorenz, F. Schein, H. von Wenckstern, *Phys. Status Solidi A* **2010**, *207*, 1437.
[2] P. D. C. King, T. D. Veal, *J. Phys.: Condens. Matter* **2011**, *23*, 334214.
[3] A. A. Husain, W. Z. Hasan, S. Shafie, M. N. Hamidon, S. S. Pandey, *Renew. Sustain. Energy Rev.* **2018**, *94*, 779.
[4] E. Fortunato, D. Ginley, H. Hosono, D. C. Paine, *MRS Bull.* **2007**, *32.3*, 242.
[5] B. K. Meyer, A. Polity, D. Reppin, M. Becker, P. Hering, P. J. Klar, T. Sander, C. Reindl, J. Benz, M. Eickhoff, C. Heiliger, M. Heinemann, J. Bläsing, A. Krost, S. Shokovets, C. Müller, C. Ronning, *Phys. Status Solidi B* **2012**, *249*, 1487.
[6] B. Kramm, A. Laufer, D. Reppin, A. Kronenberger, P. Hering, A. Polity, B. K. Meyer, *Appl. Phys. Lett.* **2012**, *100*, 094102.
[7] K. P. Hering, R. E. Brandt, B. Kramm, T. Buonassisi, B. K. Meyer, *Energy Proc.* **2014**, *44*, 32.
[8] J. Brehm, *Synthese und Charakterisierung nanokristalliner transparenter Halbleiteroxide*. Cuvillier-Verlag, Göttingen **2005**, p. 3.
[9] T. Minami, Y. Nishi, T. Miyata, *Appl. Phys. Express* **2013**, *6*, 044101.
[10] H. H. Tippins, *Phys. Rev.* **1965**, *140*, A316.
[11] M. Orita, H. Ohta, M. Hirano, H. Hosono, *Appl. Phys. Lett.* **2000**, *77*, 4166.
[12] H. He, R. Orlando, M. A. Blanco, R. Pandey, E. Amzallag, I. Baraille, M. Rérat, *Phys. Rev. B* **2006**, *74*, 195123.
[13] H. V. Wenckstern, *Adv. Electron. Mater.* **2017**, *3*, 1600350.
[14] S. Sampath Kumar, E. J. Rubio, M. Noor-A-Alam, G. Martinez, S. Manandhar, V. Shutthanandan, *J. Phys. Chem.* **2013**, *117*, 4194.
[15] K. Ishibashi, R. Aida, M. Takahara, J. Kudo, I. Tsunoda, K. Takakura, T. Nakashima, M. Shibuya, K. Murakami, *Phys. Status Solidi C* **2013**, *10*, 1588.
[16] M. Passlack, E. F. Schubert, W. S. Hobson, M. Hong, N. Moriya, S. N. G. Chu, K. Konstadinidis, J. P. Mannaerts, M. L. Schnoes, G. J. Zydzik, *J. Appl. Phys.* **1995**, *77*, 686.
[17] P. Marie, X. Portier, J. Cardin, *Phys. Status Solidi A* **2008**, *205*, 1943.
[18] E. G. Villora, K. Shimamura, K. Kitamura, K. Aoki, *Appl. Phys. Lett.* **2006**, *88*, 031105.
[19] K. Sasaki, A. Kuramata, T. Masui, E. G. Villora, K. Shimamura, S. Yamakoshi, *Appl. Phys. Express* **2012**, *5*, 035502.
[20] M. Kracht, A. Karg, J. Schlörmann, M. Weinhold, D. Zink, F. Michel, M. Rohnke, M. Schowalter, B. Gerken, A. Rosenauer, P. J. Klar, J. Janek, M. Eickhoff, *Phys. Rev. Appl.* **2017**, *8*, 054002.
[21] N. M. Sbrockey, T. Salagaj, E. Coleman, G. S. Tompa, Y. Moon, M. S. Kim, *J. Electron. Mater.* **2015**, *44*, 1357.
[22] M. Orita, H. Hiramatsu, H. Ohta, M. Hirano, H. Hosono, *Thin Solid Films* **2002**, *411*, 134.
[23] Y. Li, A. Trinchi, W. Wlodarski, K. Galatsis, K. K. Zadeh, *Sens. Actuators B* **2003**, *93*, 431.
[24] Y. Kokubun, K. Miura, F. Endo, S. Nakagomi, *Appl. Phys. Lett.* **2007**, *90*, 031912.
[25] E. Auer, A. Lugstein, S. Loffler, Y. J. Hyun, W. Brezna, E. Bertagnolli, P. Pongratz, *Nanotechnology* **2009**, *20*, 434017.
[26] T. Terasako, H. Ichinotani, M. Yagi, *Phys. Status Solidi C* **2015**, *12*, 985.
[27] S. Rafique, L. Han, H. Zhao, *Phys. Status Solidi A* **2016**, *213*, 1002.
[28] L. Jianjun, Y. Jinliang, S. Liang, L. Ting, *J. Semicond.* **2010**, *31*, 103001.
[29] H. C. Kang, *Mater. Lett.* **2014**, *119*, 123.
[30] C. V. Ramana, E. J. Rubio, C. D. Barraza, A. Miranda Gallardo, S. McPeak, S. Kotru, J. T. Grant, *J. Appl. Phys.* **2014**, *115*, 043508.
[31] J. Castillo, R. Garcia-Perez, H. Huq, *J. Electron. Mater.* **2019**, *48*, 536.
[32] T. Oshima, T. Okuno, S. Fujita, *Jpn. J. Appl. Phys.* **2007**, *46*, 7217.
[33] F. B. Zhang, K. Saito, T. Tanaka, M. Nishio, Q. X. Guo, *J. Cryst. Growth* **2014**, *387*, 96.
[34] M. Rebien, W. Henrion, M. Hong, J. P. Mannaerts, M. Fleischer, *Appl. Phys. Lett.* **2002**, *81*, 250.
[35] I. Baía, M. Quintela, L. Mendes, P. Nunes, R. Martins, *Thin Solid Films* **1999**, *337*, 171.
[36] M. Ahmadipour, S. N. Ayub, M. F. Ain, Z. A. Ahmad, *Mater. Sci. Semicond. Process.* **2017**, *66*, 157.
[37] J. Tauc, R. Grigorovici, A. Vancu, *Phys. Status Solidi* **1966**, *15*, 627.
[38] H. Nalwa, *Deposition and Processing of Thin Films*, Academic Press, San Diego **2002**, p. 416.
[39] A. Bikowski, T. Welzel, K. Ellmer, *Appl. Phys. Lett.* **2013**, *102*, 242106.
[40] H. Salmang, H. Scholze, *Keramik* (Hrsg. R. Telle), Springer-Verlag Berlin, Heidelberg, New York **2007**.

© 2019 WILEY-VCH Verlag GmbH & Co. KGaA, Weinheim

7.2 Progress in sputter-growth of β-Ga_2O_3 by applying pulsed-mode operation

Published in Phys. Status Solidi A **2020**, *217*, 1901009 [Sch20]

Clarification of my own contribution to the publication:

I developed the deposition process and deposited the majority of the samples. The X-ray diffraction, optical transmittance and relative specular reflectance, Raman spectroscopy as well as scanning electron microscopy measurement were performed by myself, whereas the atomic force microscopy as well as the transmission electron microscopy measurements were done by my co-authors. I interpreted and discussed the results with my co-authors and finally wrote the manuscript.

physica status solidi pss a
www.pss-a.com

Check for updates

Progress in Sputter Growth of β-Ga_2O_3 by Applying Pulsed-Mode Operation

Philipp Schurig, Fabian Michel, Andreas Beyer, Kerstin Volz, Martin Becker, Angelika Polity, and Peter J. Klar*

β-Ga_2O_3 thin films are deposited by pulsed radio-frequency (RF) magnetron sputtering on c-sapphire substrates, using a stoichiometric Ga_2O_3 target and a constant gas flux of an argon–oxygen mixture. Pulsed sputtering offers a way to overcome the restrictions of conventional sputtering. The parameters RF power and pulse duty cycle (PDC) are varied systematically to optimize the synthesis of Ga_2O_3 thin films. Subsequently, the resulting as-deposited (AD) Ga_2O_3 layers are analyzed in terms of structural and optical properties and the results are compared with those on the samples treated by postdeposition rapid thermal annealing. Based on this analysis, the process parameters are evaluated in terms of β-Ga_2O_3 formation. Postdeposition temperature treatments are found to yield a better crystal quality. However, a strong interdiffusion with the Al_2O_3 substrate is observed. The optical bandgap of the sputtered thin films is found to be quite independent of the RF sputtering power but to depend strongly on the PDC used, whereas the layer thickness rather strongly increases with both of those growth parameters. These evolutions are assigned to changes in the energy and ionic species of the plasma. Traces of GaO_x-related phases in addition to β-Ga_2O_3 are found in the interphase between the growing thin films and the underlying substrate.

1. Introduction

The quest for solar cell devices significantly contributing to satisfying the world's energy demand is on.[1–3] However, the only way to enable photovoltaics to fulfill the requirements of green energy and overcome the limitations of resource criticality is to use semiconducting materials, which consist of chemical elements of high abundance. The different oxide phases of copper belong to this class of materials being sustainable and nontoxic. In particular, p-type cuprous oxide is of great interest, among others, as absorber materials in heterojunction solar cell devices in contact with n-type semiconductor window layers.[4–8] The term "window material" results from the fact that the radiation initially passes through this material virtually without interaction and is absorbed subsequently from the absorber layer. In addition to wide-band-gap nitride semiconductors such as GaN (3.4 eV)[9] and $Al_xGa_{1-x}N$ (3.4 – 3.75 eV)[10] or oxides such as ZnO (3.3 eV),[9] a material, very well suited for such devices as a window layer, might be gallium sesquioxide, Ga_2O_3. This material exhibits five different confirmed phases (α, β, γ, δ, and ε). Its polymorphism was first reported by Roy et al. as early as 1952.[11] Nowadays, research on this binary oxide is still very active, as there are a wide range of possible applications, especially for the thermodynamically most stable phase β-Ga_2O_3. In addition to the aforementioned heterojunction solar cell devices, the main reasearch topics include optoelectronic devices like light emitting diodes[12] and UV photodetectors,[13,14] electronic devices like field-effect transistors[15] and Schottky barrier diodes,[16–18] or devices for sensing gases[19,20] and radiation.[21,22] The prerequisite for the reliability and good performance of such devices is a reproducible material quality assured by standardized preparation procedures. For example, the electron concentration has to be controlled by defined synthesis conditions and postdeposition thermal annealing or doping. Native point defects in β-Ga_2O_3 are gallium vacancies, both on tetrahedral and octahedral lattice sites, and three different types of oxygen vacancies. However, residual impurities are needed to explain the electrical properties observed.[23] Doping with elements like Si, Ge, and Sn on Ga sites or F on oxygen sites is feasible to establish n-type conduction.[24–26] Due to the intensive research particularly in the context of power devices, several review articles have emerged on gallium oxides and their properties.[27–32]

Synthesis of bulk Ga_2O_3 is well established. By far the largest number of publications deal with β-Ga_2O_3 and certain aspects of its versatility. Crystals of a high structural quality are available.

P. Schurig, F. Michel, Dr. M. Becker, Dr. A. Polity, Prof. P. J. Klar
Institute for Experimental Physics I and Center for Materials Research (LaMa)
Justus Liebig University Giessen
Heinrich-Buff-Ring 16, 35392 Giessen, Germany
E-mail: martin.becker@exp1.physik.uni-giessen.de

Dr. A. Beyer, Prof. K. Volz
Institute of Physical Chemistry and Materials Science Center
Philipps-University Marburg
Hans-Meerwein-Straße 6, 35032 Marburg, Germany

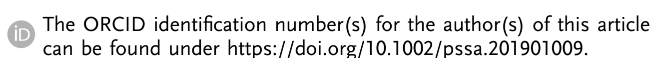
The ORCID identification number(s) for the author(s) of this article can be found under https://doi.org/10.1002/pssa.201901009.

© 2020 The Authors. Published by WILEY-VCH Verlag GmbH & Co. KGaA, Weinheim. This is an open access article under the terms of the Creative Commons Attribution-NonCommercial-NoDerivs License, which permits use and distribution in any medium, provided the original work is properly cited, the use is non-commercial and no modifications or adaptations are made.

DOI: 10.1002/pssa.201901009

They can be produced by gas phase and flux growth techniques, as well as melt growth methods, which present a main technological advantage compared with other wide-bandgap materials of industrial importance, i.e., gallium nitride and silicon carbide. Although different kinds of bulk growth techniques in different environments exist, nowadays, melt growth techniques dominate due to the industrial applicability on large scale.[31,32] Demonstrably, the Czochralski method,[33,34] edge-defined film-fed growth (EFG),[35] and vertical Bridgman (VB) methods[36] are capable of fulfilling the need of upscaling. For example, EFG can be used to produce even 4 inch-diameter single-crystal wafers.[37] Thin films can be realized by a variety of techniques, chemical vapor deposition (CVD),[38–41] metal-organic chemical vapor deposition (MOCVD),[42] molecular beam epitaxy (MBE),[43–48] pulsed laser deposition (PLD),[5,49–51] and sol–gel synthesis,[52–55] among others. A topical review with focus on the progress in the synthesis of bulk as well as thin films of Ga_2O_3 was recently given by Galazka.[32]

As growth conditions or postgrowth annealing parameters influence layer properties like degree of crystallinity, composition, or morphology, among others, each deposition method has its own right to exist depending on the application sought for. The main objective, however, is to bring in line the material properties with economic and financial efficiency. Therefore, an increase in the growth rate is often required to ensure use on an industrial scale. In those cases, sputtering techniques seem to be viable candidates for achieving this goal.[56,57] Atoms ejected from the target's surface by energetic ion impingement are neutral unless they are ionized, inter alia, by application of very high power to the discharge.[58] The target power density, however, is limited owing to target heating. Hence, obtaining thin layers of an insulating material with low defect densities and high compactness is very challenging. The process is mainly hampered by the occurrence of arc events at the target, however, pulsing the magnetron discharge has been found to stabilize the reactive sputtering process. In pulsed DC deposition systems glow discharges with a target power density of up to 900 $W\,cm^{-2}$ have been obtained.[59] Thus, switching from standard to the pulsed mode at constant target power is promising to overcome the main challenge in obtaining crystalline β-Ga_2O_3, namely acquiring the secondary particle energy necessary for growth along a preferential crystal orientation. However, literature concerning the influence of the additional sputter parameters, e.g. pulse duty cycle (PDC) or pulse repetition frequency (PRF), on metal oxide growth is still scarce.

In this work, we discuss the sputter deposition of Ga_2O_3 thin films on c-sapphire substrates using radio-frequency (RF) magnetron sputtering in the pulsed mode and compare the layers obtained with thin films deposited by conventional RF magnetron sputtering. Sputtering power as well as PDC was varied. Additionally, the influence of a postdeposition thermal annealing step is investigated. Subsequently, the Ga_2O_3 films were analyzed to identify a suitable growth window for β-Ga_2O_3.

2. Experimental Section

Ga_2O_3 thin films were grown on *c*-plane sapphire substrates by conventional RF magnetron sputtering at 13.56 MHz. The substrates were cleaned with acetone and methanol in an ultrasonic bath, dried with nitrogen, and mounted in the sputter chamber (base pressure of 5×10^{-7} mbar) subsequently. In the growth process, a plasma of the process gas was generated between the target and the substrate. Ions of the process gas, in our case, a mixture of inert argon and reactive molecular oxygen (ratio 4:1), impinged onto a target, here, a Ga_2O_3 ceramic target and sputter-off target atoms. These atoms along with the reactive species of the process gas formed an oxide film on the substrate. The RF power coupled into the plasma was generated by a "Dressler CESAR 1312" system equipped with a "Dressler VM 1500 AW" matching network. Additionally, the regular sputtering mode of the very same RF power generator was superimposed by a selected frequency scheme. Utilizing this mode of operation additional parameters may be varied. Most importantly, the PDC, the on-to-off ratio of sputter time, was changed between 10% and 70%.

The growth temperature was kept constant at 650 K based on measuring the temperature with a thermocouple. The temperature, the actual growth temperature (surface temperature), was expected to be considerably higher, depending on the RF power coupled into the plasma, the target-substrate geometry, and the target's thermal conductivity. The temperature range was chosen in accordance with the findings of Akazawa and Zhang et al., who observed the threshold temperature of crystalline Ga_2O_3 at 500 and 300 °C, respectively.[56,60] Details on the distinct temperature characteristics of the setup can be found elsewhere.[57]

Here, we discuss two series of samples. Throughout each series a specific process parameter was varied systematically, whereas all the other process parameters were kept constant, cf. **Table 1**. The variables chosen were RF sputter power in series I and PDC in series II. Thus, series I resembled conventional RF sputter deposition at fixed PRF and PDC values, whereas series II illustrated the impact of using the pulsed mode in the sputter deposition of β-Ga_2O_3. The results of the series were compared with measurements conducted on samples which were conventionally sputtered using the same setup and reported previously.[57] All samples were unintentionally doped and, thus, did not show significant electrical conductivity, which was most likely driven by the pronounced grain structure intrinsic for sputtered thin films.

After all as-deposited (AD) samples were measured, and a rapid thermal annealing process was conducted on all specimens. The samples were treated at 1000 °C for 1 h in ambient atmosphere. All as-grown Ga_2O_3 films as well as all annealed specimens were analyzed by X-ray diffraction (Siemens D 5000) in a Bragg–Brentano $\Theta - 2\Theta$ geometry. Optical transmittance at normal incidence ($\beta = 0°$) and relative specular reflectance close to normal incidence ($\beta = 6°$) were recorded using a "PerkinElmer Lambda 900" spectrometer. The influence of the substrate was eliminated by measuring a substrate baseline prior to thin-film deposition. The morphology of the sample surfaces

Table 1. Parameters used in the pulsed sputter processes for depositing sample series I and II.

Series	RF power [W]	PDC [%]	PRF [kHz]	Plasma on-time [min]
I	600–1000	10	1	6
II	800	10–70	1	6

32

© 2020 The Authors. Published by WILEY-VCH Verlag GmbH & Co. KGaA, Weinheim

was studied by scanning electron microscopy (SEM) and atomic force microscopy (AFM), using a Zeiss MERLIN scanning electron microscope equipped with an In-Lens detector and an AIST-NT SmartSPM operating in the noncontact mode. Raman spectra with a spectral resolution of 1.5 cm^{-1} were acquired with a Renishaw inVia Raman microscope system using 514 nm laser excitation. Electron-transparent samples were prepared using a JEOL JIB-4601F dual beam system operating at 3–30 kV. Thin protective layers of carbon and tungsten were deposited by the electron beam-assisted deposition on the surface of the thin film. This was followed by 2 μm thick carbon and tungsten layer deposition using the Ga ion beam. This procedure was chosen to not damage the surface with impinging Ga ions during initial growth. A cross-sectional sample was produced by thinning down the sample from the substrate side to 500 nm with a 30 kV ion beam and then to 300 and 200 nm using a 15 and 10 kV ion beam, respectively. Finally, the material was thinned to about 100 nm with 5 kV ions and polishing was done with a 3 kV ion beam to remove the damaged layer. Transmission electron microscopy (TEM) characterization, i.e. the acquisition of high-resolution images as well as selected-area electron diffraction (SAED) patterns, was conducted in a JEOL JEM 3010 operating at 300 kV.

3. Results and Discussion

First, we will recap tendencies observed in the conventional RF sputter deposition of Ga_2O_3.[57] The optical bandgap strongly depends on the deposition parameters oxygen flux, heating power, and RF power. Polycrystalline β-Ga_2O_3 with an optical bandgap and a refractive index close to the values of bulk material was obtained under oxygen excess at a low RF power and relatively moderate growth temperatures of about 600 °C. The general trend of the optical bandgaps depending on RF sputtering power is explained as follows. Less kinetic energy of the process gas ions impinging on the target results from a lower RF power coupled into the plasma. Excess oxygen is required to compensate the excess of Ga due to preferential sputtering in the particle flux toward the substrate.[61] In summary, at the fixed gas flux ratio, increasing the RF power was found to influence the optical parameters the most. An increase in growth temperature resulted in an enhanced crystal quality and a composition tending toward stoichiometry. Unfortunately, the conventional RF magnetron sputter setup is limited in further increasing heating power and lowering RF power and, thus, achieving higher crystallinity.

A common way to overcome this drawback is to perform post-deposition temperature treatment. Crystallinity might be enhanced by heating the films, as atoms on the lattice may rearrange and oxygen vacancies or interstitials may be removed, depending on the surrounding atmosphere. However, we found that in the case of heterostructures of Ga_2O_3 and Al_2O_3 (sapphire), strong interdiffusion occurs at the high annealing temperatures of about 1000 °C. We found by secondary-ion mass spectrometry measurements that after annealing for 1 h, the Al content in the Ga_2O_3 films is increased by almost two orders of magnitude, corresponding to atomic fractions in the order of percent, cf. Supporting Information.

Thus, an alternative way has to be sought for improving the layer quality. To circumvent the restrictions of the conventional continuous sputtering process, we switch to a pulsed operation. In doing so, the sputtering power might be further enhanced to effectively yield higher growth temperatures. Similar to conventional RF sputtering the increase in applied RF power should enhance the primary particle energy and, thus, the particles' ability to sputter target atoms. Consequently, it is assumed that the grown oxide layers are thicker and of enhanced crystallinity.

Figure 1 shows the results for series I, in which the RF sputtering power was varied for fixed PRF and PDC values of 1 kHz and 10%, respectively. The layer thicknesses linearly increase with the RF sputtering power from 300 to 700 nm, cf. Figure 1a. However, they do not change much after annealing. The error margins shown originate from the uncertainty of the refractive index value used in thickness determination.[43] The layer

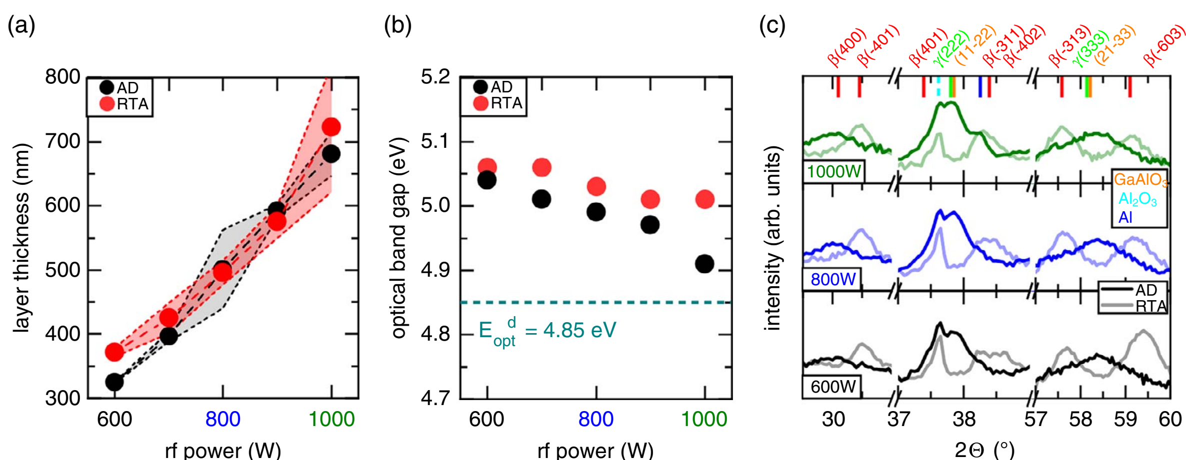

Figure 1. a) Layer thickness and b) optical bandgap of AD and rapid thermal annealed (RTA) Ga_2O_3 layers deposited on *c*-plane sapphire by varying the pulsed RF sputtering power. Error margins given in (a) arise due to the uncertainty of the refractive index used in the analysis.[43] While the layer thickness is not affected significantly by the thermal annealing procedure, the optical bandgaps exceed in this sputter series, most likely due to the Al interdiffusion. c) X-ray diffractograms for selected samples, deposited at 600, 800 and 1000 W, respectively. Although there is no significant influence of the RF power for AD samples, slight changes in the reflection ratios might be detected for the annealed samples.

© 2020 The Authors. Published by WILEY-VCH Verlag GmbH & Co. KGaA, Weinheim

thicknesses obtained translate to growth rates of around 50–120 nm min^{-1} plasma on-time. Compared with the growth rate of approximately 4–5 nm min^{-1} found for conventionally sputtered layers,[57] this is a significant improvement.

The optical bandgaps of the samples of series I are shown in Figure 1b. The samples grown at the highest RF power exhibit optical bandgaps closest to values reported for stoichiometric β-Ga_2O_3.[62,63] At first glance, this seems contradictory to what was obtained for conventionally sputtered samples, where the lowest RF power yielded optical bandgaps closest to the theoretical value for stoichiometric β-Ga_2O_3.[57] However, the general trend of the optial bandgap values of Ga_2O_3 with increasing RF sputtering power is the same, as they significantly decrease in a linear fashion from 5.1 to 4.9 eV. Thus, we tentatively assign the cause of the findings in Figure 1b to be a superposition of two effects: first, the effect of RF sputter power on the preferential sputtering being the same, as shown for conventional sputtering, and the overall shift of this tendency to higher bandgaps triggered by the pulsed operation. Thus, a careful tuning of RF sputtering power and oxygen flux being intertwined is necessary to yield bulk material's optical bandgap.

After rapid thermal annealing the optical bandgaps obtained for the Ga_2O_3 layers increased compared with those of the AD samples. We ascribe this enhancement to the diffusion of Al from the sapphire substrate into the Ga_2O_3 layer. Thus, metastable phases like $(Ga,Al)O_3$ might be present in the polycrystalline structure. Additionally, there seems to be a saturation at optical bandgaps of around 5.0 eV for the annealed samples. As Al and Ga are chemically similar, it is possible to substitute either easily by the other.[64,65] However, with increasing sputtering power, which translates to a larger layer thickness, this effect slowly becomes less important as the layer thickness exceeds the maximum diffusion length of Al in Ga_2O_3 at 1000 °C reached after 1 h.

Figure 1c shows X-ray diffractograms for selected samples, deposited at 600, 800, and 1000 W, respectively, in the AD state (bold) as well as after postdeposition thermal treatment (transparent). The AD layers exhibit broad peaks of low intensities at about 30°, 38°, and 58.5°, which may be assigned to the reflections (400), (−313), and (−603) β-Ga_2O_3, although being shifted compared with the literature values of bulk material. However, a trustworthy assignment is rather difficult, as reflections of other gallium oxide phases like γ-Ga_2O_3 or even metastable phases like $(Ga,Al)O_3$ might be superimposed.

In principle, α-phase Ga_2O_3 shows a better lattice match with *c*-plane sapphire than its β-phase. However, β-phase Ga_2O_3 is more commonly observed when growth occurs on this kind of substrate, presumably due to its lower chemical potential.[56,57] Furthermore, surface roughness and defect density on the substrate surface affect the growth conditions and, thus, the crystallization of different phases.[56,60,66] For example, a shift from β-phase to γ-phase was observed when growing in an environment containing water vapor, detrimental for the formation of high-temperature phases.[56] Thus, we expect the diffractogram to change significantly after carrying out postgrowth thermal treatment. Indeed, after annealing the reflections shift significantly or even vanish completely. While the untreated layers are mainly amorphous, at least what can be deduced from X-ray diffraction, with exception of broad peaks not to be assigned to a distinct plane or phase, annealed samples show different out-of-plane orientations of the β-phase and may be considered polycrystalline. In particular, the (−401) and (−313) reflections of β-Ga_2O_3 appear, whereas reflections of the {−h01} family of planes shift toward the value of bulk material. This is in line with the findings of Roy et al. that gallium oxide transforms into the β-phase at elevated temperatures, no matter which phase had been present beforehand.[11] Another hint can be found when comparing the samples grown in the pulsed mode with those sputtered in the non-pulsed fashion. While the former shows reflections presumably corresponding to a superposition of various phases, the latter clearly exhibits β-Ga_2O_3, although slightly strained.[57]

Thus, we suspect pulsed-mode sputtering to support the synthesis of mixed-phase samples which then vanish under postgrowth thermal treatment. Especially the rather strong contributions of reflections, tentatively assigned to γ-Ga_2O_3, disappear. Similar to the α-phase the thermodynamic stability of the γ-phase is only metastable and changes into the β-phase above 650 °C.[11]

Series II was deposited at different PDCs, cf. Table 1, to clarify its impact on the thin-film growth. A PDC of 100% corresponds to conventional RF sputter deposition. Thus, increasing the PDC leads to prolonged sputter pulses and thus to higher plasma on-times. To detach an influence of the PDC itself from an influence of increased plasma on-times, the total plasma on-time was kept constant by reducing the overall sputter time.

Figure 2a shows the dependence of layer thickness as a function of the PDC. The values obtained increase nonlinearly between 0.5 and 2.6 μm with the highest slope in the intermediate range between 40% and 50% PDC. We tentatively assign this evolution to changes in the energy and species of the plasma ions. Keeping the RF sputtering power constant, the increase in PDC is synonymous with the increase in on-time in which the ions are accelerated. As a consequence, changing the PDC value will affect the energy distribution, species, and cross sections of dominant primary ions and, as a consequence, the properties of the secondary target particles can be manipulated.[67] Thus, inter alia, the timescale for ordering at the substrate surface is modified. Sputtered species may have gained enough energy to statistically evaporate after arriving at the substrate surface, resulting in a saturation behavior of the remaining layer thickness. Additionally, it is known that pulsed-mode sputtering increases the rate of negatively charged oxygen atoms, which may impinge on the surface of the growing layer and induce surface etching, resulting in reduced layer thickness. Analysis of the distribution of plasma species and their impact on the overall process is ongoing.

The corresponding optical bandgaps versus PDC are shown in Figure 2b. With increasing PDC value the optical bandgaps decrease until they reach values around 4.65 eV. Below the optical bandgap of bulk β-Ga_2O_3 the decrease might be explained by an increased defect density caused by less time for the atomic species to a suitable order on the substrate surface at high PDC. Accordingly, for a given frequency, the PDC value has to be optimized for a given sputtering power.

It should be noted that the annealing process has very limited influence on both the layer thickness and the optical bandgaps. If any, there is a deviation of the optical bandgaps of layers

© 2020 The Authors. Published by WILEY-VCH Verlag GmbH & Co. KGaA, Weinheim

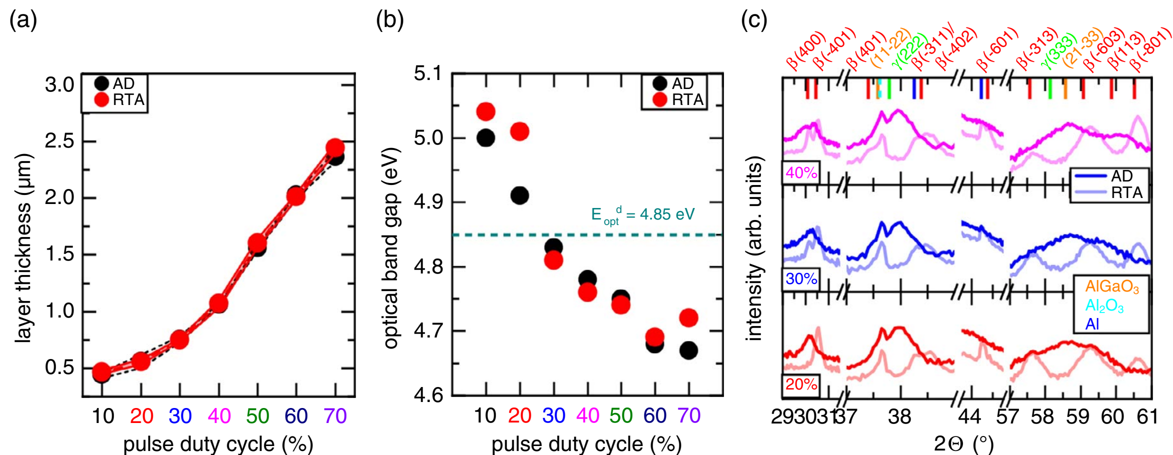

Figure 2. a) Layer thickness and b) optical bandgap of the AD and RTA Ga_2O_3 layers deposited on *c*-plane sapphire by varying the PDC. Error margins given in (a) arise due to the uncertainty of the refractive index used in the analysis.[43] c) X-ray diffractograms for selected samples, deposited at 20%, 30%, and 40% PDC, respectively.

grown at low PDCs. Here, the higher bandgaps of annealed samples might again well be attributed to Al diffusion into the Ga_2O_3, as this effect is known to be more significant for thinner samples. One might even think of alloying in the vicinity of the substrate, resulting in the $GaAlO_3$ spinel. More insight into this is given by the structural analysis. In this context, Figure 2c shows the diffractogram of the layers deposited at 20%, 30%, and 40% PDC, respectively. The AD layers are shown in bold colors and the thermally treated samples in transparent colors. Comparing the data with the diffractograms shown in Figure 1c, no significant changes can be observed. So the general trend of pulsed-mode sputtering to support the synthesis of mixed-phase samples which then vanish under postgrowth thermal treatment still holds. Thus, the broad reflections at 38° and 58.5° most likely represent the (222) and (333) reflection of γ-Ga_2O_3. Due to the overall low crystalline quality, however, one has to assume rather small γ-Ga_2O_3 domains in an amorphous matrix. After thermal annealing the γ-Ga_2O_3 peaks vanish due to phase transformation to the β-phase, taking place above 650 °C. Thus, all reflections observed in the annealed layers may be interpreted as β-Ga_2O_3, confirming better crystalline quality. However, there also exist minor differences compared with the results shown in Figure 1c. One such difference is the appearance of additional or at least more pronounced reflections for the annealed samples around 30°, 44°, and 60.5°. All these reflections belong to the $\{-h01\}$ family of planes and increase in relative intensity when the PDC is increased. It seems that the $\{-h01\}$ family of planes exhibits a comparatively high formation energy, which is delivered only at higher duty cycles.

To further evaluate the actual crystallinity of a representative pulsed sputtered Ga_2O_3 thin film, we will now focus on the sample grown at 800 W RF sputter power and 30% PDC. **Figure 3** shows a) the corresponding Raman spectra of the annealed layer in comparison with those of an untreated layer and a sapphire substrate as references, as well as the surface morphology of the annealed and as-grown Ga_2O_3 samples measured by b) SEM and c) AFM. Although it is beyond this article to evaluate the data in detail, both Raman spectra and the surface morphology investigated via SEM and AFM, respectively, confirm a more pronounced crystallinity after annealing.[68] Especially Raman spectroscopy is known to very sensitively differentiate material phases[48,69,70] or locate defect structures.[71] Thus, the presumption of the conversion of amorphous material into β-Ga_2O_3 throughout the discussion is further underlined.

Additionally, TEM measurements were carried out, cf. Figure 3d–f, especially to investigate the interface region between the Ga_2O_3 layer and the Al_2O_3 substrate. Figure 3d shows the SAED pattern obtained from a thin slice of a thin film deposited at 30% PDC. The circles in the pattern indicate polycrystalline material.[72] Therefore, the SAED pattern underlines the findings of the XRD measurement in that polycrystalline domains in an amorphous matrix are present. A cross-sectional TEM view, cf. Figure 3e, enables a distinction between the polycrystalline and amorphous domains and even differently oriented domains. However, the most striking feature is the possibility to investigate the interface region, cf. Figure 3f. It should be noted that the interface appears to be smeared out, indicating slight interdiffusion. As the measurements shown represent an as-grown sample, this is most likely an effect of the impingment of negatively charged oxygen ions.[73] Nevertheless, the structure of the substrate continues for some nm in the Ga_2O_3 layer, replacing Al atoms by Ga atoms (a brighter impression). Thus, we tentatively assign this pseudomorphous grown region as γ-Ga_2O_3.

It should be noted that α-Ga_2O_3 might also be observed at the interface with sapphire.[74,75] Phase stabilization of α-Ga_2O_3 was observed on *r*-plane α-Al_2O_3 in plasma-assisted MBE up to a film thickness of around 200 nm.[76] Thus, initially the resulting strain energy due to lattice mismatch shifts the thermodynamic equilibrium from the stable β-Ga_2O_3 toward the metastable α-modification.[77] However, for increasing growth times, nucleation of β-phase was found on the *c*-plane facets of α-Ga_2O_3. Here, we do not see any indication of the α-phase being present in the interface, although we cannot rule out entirely the presence of some domains.

© 2020 The Authors. Published by WILEY-VCH Verlag GmbH & Co. KGaA, Weinheim

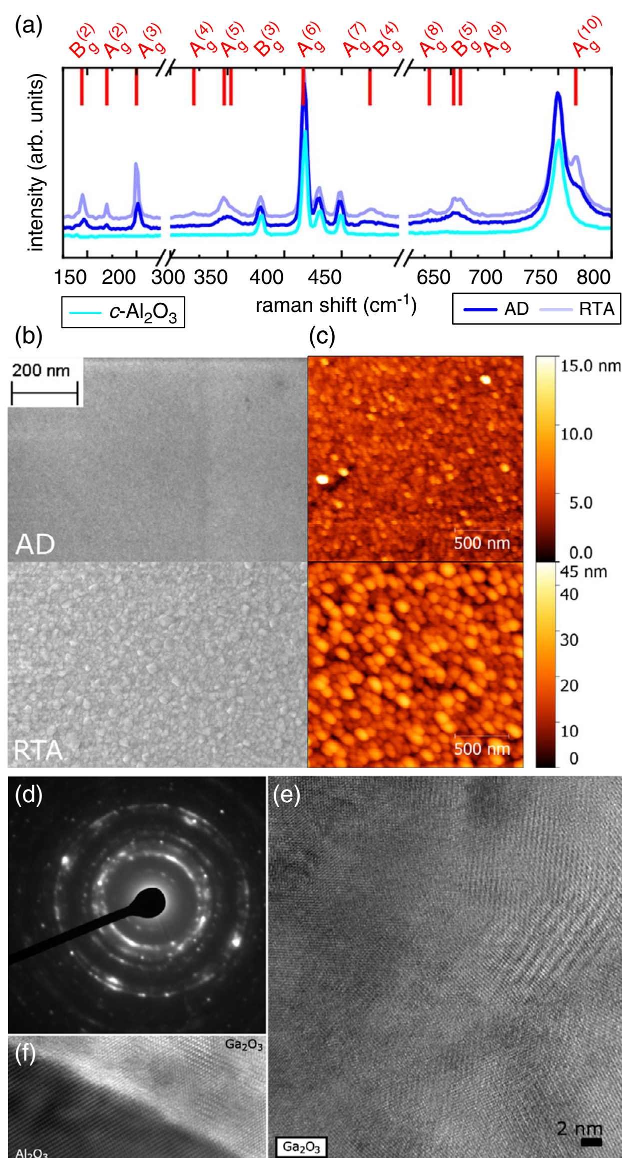

Figure 3. (a) Raman spectra of a representative pulsed-sputtered Ga_2O_3 thin film, grown at 800 W RF sputter power and 30% PDC. The theoretical mode positions displayed earlier were taken from Kranert et al.[78] b) SEM and c) AFM measurements of annealed samples in comparison with an as-deposited layer. An increase in temperature is accompanied by an increased amount of crystalline phase. d) SAED pattern, e) cross-sectional TEM, and f) HRTEM measurement of the interface region between the Ga_2O_3 layer and the Al_2O_3 substrate for the AD sample grown at 800 W RF sputter power and 30% PDC.

4. Conclusions

Thin films of β-Ga_2O_3 were deposited by pulsed RF magnetron sputtering on c-sapphire substrates. The growth rates were significantly increased compared with those measured for conventionally sputtered β-Ga_2O_3 layers. The optical bandgap of the sputtered thin films was found to be quite independent of the RF sputtering power but to depend strongly on the PDC, whereas the layer thickness rather strongly increased with both of those growth parameters. We tentatively assign these evolution to changes in the energy and species of the plasma ions. However, the overall crystal quality of β-Ga_2O_3 is still in need of improvement, which we assign to the presence of other GaO_x-related phases at the interphase between β-Ga_2O_3 and the underlying substrate.

Supporting Information

Supporting Information is available from the Wiley Online Library or from the author.

Acknowledgements

Financial support was provided by the Deutsche Forschungsgemeinschaft (DFG) via the Research Training Group (RTG) 2204 "Substitute Materials for sustainable Energy Technologies".

Conflict of Interest

The authors declare no conflict of interest.

Keywords

gallium oxide, pulsed radio-frequency magnetron sputter deposition, structures, thin films

Received: December 4, 2019
Revised: February 10, 2020
Published online:

[1] A. Feltrin, A. Freundlich, *Renew. Energy* **2008**, *33*, 180.
[2] C. Wadia, A. P. Alivisatos, D. M. Kammen, *Environ. Sci. Technol.* **2009**, *43*, 2072.
[3] T. Unold, H. W. Schock, *Annu. Rev. Mater. Res.* **2011**, *41*, 297.
[4] B. K. Meyer, A. Polity, D. Reppin, M. Becker, P. Hering, P. J. Klar, T. Sander, C. Reindl, J. Benz, M. Eickhoff, C. Heiliger, M. Heinemann, J. Bläsing, A. Krost, S. Shokovets, C. Müller, C. Ronning, *Phys. Status Solidi B* **2012**, *249*, 1487.
[5] T. Minami, Y. Nishi, T. Miyata, *Appl. Phys. Express* **2013**, *6*, 044101.
[6] T. Minami, Y. Nishi, T. Miyata, *Appl. Phys. Express* **2015**, *8*, 022301.
[7] T. Minami, Y. Nishi, T. Miyata, *Appl. Phys. Express* **2016**, *9*, 052301.
[8] Y. S. Lee, D. Chua, R. E. Brandt, S. C. Siah, J. V. Li, J. P. Mailoa, S. W. Lee, R. G. Gordon, T. Buonassissi, *Adv. Mater.* **2014**, *26*, 4704.
[9] B. Kramm, A. Laufer, D. Reppin, A. Kronenberger, P. Hering, A. Polity, B. K. Meyer, *Appl. Phys. Lett.* **2012**, *100*, 094102.
[10] F. Michel, B. Kramm, M. Becker, K. P. Hering, D. M. Hofmann, P. J. Klar, *J. Appl. Phys.* **2018**, *123*, 245304.
[11] R. Roy, V. G. Hill, E. F. Osborn, *J. Am. Chem. Soc.* **1952**, *74*, 719.
[12] D. Li, V. Hoffmann, E. Richter, T. Tessaro, Z. Galazka, M. Weyers, G. Tränkle, *J. Cryst. Growth* **2017**, *478*, 212.
[13] T. Ohshima, T. Okuno, N. Arai, N. Suzuki, S. Ohira, S. Fujita, *Appl. Phys. Express* **2008**, *1*, 011202.
[14] M. Zhong, Z. Wei, X. Meng, F. Wu, J. Li, *J. Alloy. Compd.* **2015**, *619*, 572.
[15] M. Higashiwaki, K. Sasaki, A. Kuramata, T. Masui, S. Yamakoshi, *Appl. Phys. Lett.* **2012**, *100*, 013504.

© 2020 The Authors. Published by WILEY-VCH Verlag GmbH & Co. KGaA, Weinheim

[16] D. Splith, S. Müller, F. Schmidt, H. von Wenckstern, J. J. van Rensburg, W. E. Meyer, M. Grundmann, *Phys. Status Solidi A* **2014**, *211*, 40.
[17] S. Müller, H. von Wenckstern, F. Schmidt, D. Splith, F. L. Schein, H. Frenzel, M. Grundmann, *Appl. Phys. Express* **2015**, *8*, 121102.
[18] Q. He, W. Mu, H. Dong, S. Long, Z. Jia, H. Lv, Q. Liu, M. Tang, X. Tao, M. Liu, *Appl. Phys. Lett.* **2017**, *110*, 093503.
[19] M. Bartic, M. Ogita, M. Isai, C. Baban, H. Suzuki, *J. Appl. Phys.* **2007**, *102*, 023709.
[20] R. Pandeeswari, B. G. Jeyaprakash, *Sens. Actuators B* **2014**, *195*, 206.
[21] Y. Usui, T. Oya, G. Okada, N. Kawaguchi, T. Yanagida, *Optik* **2017**, *143*, 150.
[22] Y. Usui, D. Nakauchi, N. Kawano, G. Okada, N. Kawaguchi, T. Yanagida, *J. Phys. Chem. Solids* **2018**, *117*, 36.
[23] J. B. Varley, H. Peelaers, A. Janotti, C. G. Van de Walle, *J. Phys.: Condens. Matter* **2011**, *23*, 334212.
[24] M. Higashiwaki, K. Sasaki, T. Kamimura, M. H. Wong, D. Krishnamurthy, A. Kuramata, T. Masui, S. Yamakoshi, *Appl. Phys. Lett.* **2013**, *103*, 1.
[25] A. J. Green, K. D. Chabak, E. R. Heller, R. C. Fitch, M. Baldini, A. Fiedler, K. Irmscher, G. Wagner, Z. Galazka, S. E. Tetlak, A. Crespo, K. Leedy, G. H. Jessen, *IEEE Electron Device Lett.* **2016**, *37*, 902.
[26] E. G. Villora, K. Shimamura, Y. Yoshikawa, T. Ujiie, K. Aoki, *Appl. Phys. Lett.* **2008**, *92*, 174.
[27] M. Higashiwaki, H. Murakami, Y. Kumagai, A. Kuramata, *Jpn. J. Appl. Phys.* **2016**, *55*, 1202A1.
[28] S. I. Stepanov, V. I. Nikolaev, V. E. Bougrov, A. E. Romanov, *Rev. Adva. Mater. Sci.* **2016**, *44*, 63.
[29] H. v. Wenckstern, *Adv. Electron. Mater.* **2017**, *3*, 1600350.
[30] M. A. Mastro, A. Kuramata, J. Calkins, J. Kim, F. Ren, S. J. Pearton, *ECS J. Solid State Sci. Technol.* **2017**, *6*, P356.
[31] M. Baldini, Z. Galazka, G. Wagner, *Mater. Sci. Semicond. Proc.* **2018**, *78*, 132.
[32] Z. Galazka, *Semicond. Sci. Technol.* **2018**, *33*, 113001.
[33] Z. Galazka, K. Irmscher, R. Uecker, R. Bertram, M. Pietsch, A. Kwasniewski, M. Naumann, T. Schulz, R. Schewski, D. Klimm, M. Bickermann, *J. Cryst. Growth* **2014**, *404*, 184.
[34] Z. Galazka, R. Uecker, D. Klimm, K. Irmscher, M. Naumann, M. Pietsch, A. Kwasniewski, R. Bertram, S. Ganschow, M. Bickermann, *ECS J. Solid State Sci. Technol.* **2017**, *6*, Q3007.
[35] A. Kuramata, K. Koshi, S. Watanabe, Y. Yamaoka, T. Masui, S. Yamakoshi, *Jpn. J. Appl. Phys.* **2016**, *55*, 1202A2.
[36] K. Hoshikawa, E. Ohba, T. Kobayashi, J. Yanagisawa, C. Miyagawa, Y. Nakamura, *J. Cryst. Growth* **2016**, *447*, 36.
[37] H. Aida, K. Nishiguchi, H. Takeda, N. Aota, K. Sunakawa, Y. Yaguchi, *Jpn. J. Appl. Phys.* **2008**, *47*, 8506.
[38] G. A. Battiston, R. Gerbasi, M. Porchia, R. Bertoncello, F. Caccavale, *Thin Solid Films* **1996**, *279*, 115.
[39] E. Auer, A. Lugstein, S. Loffler, Y. J. Hyun, W. Brezna, E. Bertagnolli, P. Pongratz, *Nanotechnology* **2009**, *20*, 434017.
[40] T. Terasako, H. Ichinotani, M. Yagi, *Phys. Status Solidi C* **2015**, *12*, 985.
[41] S. Rafique, L. Han, H. Zhao, *Phys. Status Solidi A* **2016**, *213*, 1002.
[42] N. M. Sbrockey, T. Salagaj, E. Coleman, G. S. Tompa, Y. Moon, M. S. Kim, *J. Electron. Mater.* **2015**, *44*, 1357.
[43] M. Rebien, W. Henrion, M. Hong, J. P. Mannaerts, M. Fleischer, *Appl. Phys. Lett.* **2002**, *81*, 250.
[44] E. G. Villora, K. Shimamura, K. Kitamura, K. Aoki, *Appl. Phys. Lett.* **2006**, *88*, 031105.
[45] K. Sasaki, A. Kuramata, T. Masui, E. G. Villora, K. Shimamura, S. Yamakoshi, *Appl. Phys. Express* **2012**, *5*, 035502.
[46] H. Okumura, M. Kita, K. Sasaki, A. Kuramata, M. Higashiwaki, J. S. Speck, *Appl. Phys. Express* **2014**, *7*, 095501.
[47] P. Vogt, O. Bierwagen, *Appl. Phys. Lett.* **2016**, *109*, 062103.
[48] M. Kracht, A. Karg, J. Schörmann, M. Weinhold, D. Zink, F. Michel, M. Rohnke, M. Schowalter, B. Gerken, A. Rosenauer, P. J. Klar, J. Janek, M. Eickhoff, *Phys. Rev. Appl.* **2017**, *8*, 054002.
[49] M. Orita, H. Ohta, M. Hirano, H. Hosono, *Appl. Phys. Lett.* **2000**, *77*, 4166.
[50] M. Orita, H. Hiramatsu, H. Ohta, M. Hirano, H. Hosono, *Thin Solid Films* **2002**, *411*, 134.
[51] K. Matsuzaki, H. Hiramatsu, K. Nomura, H. Yanagi, T. Kamiya, M. Hirano, H. Hosono, *Thin Solid Films* **2006**, *496*, 37.
[52] T. Minami, *Solid-State Electron.* **2003**, *47*, 2237.
[53] Y. Li, A. Trinchi, W. Wlodarski, K. Galatsis, K. K. Zadeh, *Sens. Actuators B* **2003**, *93*, 431.
[54] Y. Kokubun, K. Miura, F. Endo, S. Nakagomi, *Appl. Phys. Lett.* **2007**, *90*, 031912.
[55] R. Moos, N. Izu, F. Rettig, S. Reiss, W. Shin, I. Matsubara, *Sensors* **2011**, *11*, 3439.
[56] H. Akazawa, *Vacuum* **2016**, *123*, 8.
[57] P. Schurig, M. Couturier, M. Becker, A. Polity, P. J. Klar, *Phys. Status Solidi A* **2019**, 1900385.
[58] W. M. Posadowski, *Vacuum* **1995**, *46*, 1017.
[59] R. Gruen, US Patent 5 015 493, (**1991**).
[60] F. B. Zhang, K. Saito, T. Tanaka, M. Nishio, Q. X. Guo, *J. Cryst. Growth* **2014**, *387*, 96.
[61] S. S. Kumar, E. J. Rubio, M. Noor-A-Alam, G. Martinez, S. Manandhar, V. Shutthanandan, *J. Phys. Chem.* **2013**, *177*, 4194.
[62] J. B. Varley, J. R. Weber, A. Janotti, C. G. Van de Walle, *Appl. Phys. Lett.* **2010**, *97*, 142106.
[63] C. Janowitz, V. Scherer, M. Mohamed, A. Krapf, H. Dwelk, R. Manzke, Z. Galazka, R. Uecker, K. Irmscher, R. Fornari, M. Michling, D. Schmeißer, J. R. Weber, J. B. Varley, C. G Van de Walle, *New J. Phys.* **2011**, *13*, 085014.
[64] V. G. Hill, R. Roy, E. F. Osborn, *J. Am. Ceram. Soc.* **1952**, *35*, 135.
[65] T. Oshima, T. Okuno, N. Arai, Y. Kobayashi, S. Fujita, *Jpn. J. Appl. Phys.* **2009**, *48*, 070202.
[66] T. Oshima, T. Okuno, *Jpn. J. Appl. Phys.* **2007**, *46*, 7217.
[67] J. Vlček, D. Kolenatý, J. Houška, T. Kozák, R. Čerstvý, *J. Phys. D* **2017**, *50*, 38LT01.
[68] X. Du, W. Mi, C. Luan, Z. Li, C. Xia, J. Ma, *J. Cryst. Growth* **2014**, *404*, 75.
[69] M. Becker, A. Polity, P. J. Klar, B. K. Meyer, *Phys. Status Solidi RRL* **2015**, *9*, 326.
[70] B. Eifert, M. Becker, C. T. Reindl, M. Giar, L. Zheng, A. Polity, Y. He, C. Heiliger, P. J. Klar, *Phys. Rev. Mat.* **2017**, *1*, 014602.
[71] T. Sander, C. T. Reindl, M. Giar, B. Eifert, M. Heinemann, C. Heiliger, P. J. Klar, *Phys. Rev. B* **2014**, *90*, 045203.
[72] D. B. Williams, C. B. Carter, Transmission Electron Microscopy, Sprinter-Verlag, New York **2009**.
[73] D. Severin, O. Kappertz, T. Nyberg, S. Berg, M. Wuttig, *Thin Solid Films* **2007**, *515*, 3554.
[74] D. Shinohara, S. Fujita, *Jpn. J. Appl. Phys.* **2008**, *47*, 7311.
[75] Y. Yao, S. Okur, L. A. M. Lyle, G. S. Tompa, T. Salagaj, N. Sbrockey, R. F. Davis, L. M. Porter, *Mater. Res. Lett.* **2018**, *6*, 268.
[76] M. Kracht, A. Karg, M. Feneberg, J. Bläsing, J. Schörmann, R. Goldhahn, M. Eickhoff, *Phys. Rev. Appl.* **2018**, *10*, 024047.
[77] R. Schewski, G. Wagner, M. Baldini, D. Gogova, Z. Galazka, T. Schulz, T. Remmele, T. Markurt, H. von Wenckstern, M. Grundmann, O. Bierwagen, P. Vogt, M. Albrecht, *Appl. Phys. Express* **2015**, *8*, 011101.
[78] C. Kranert, C. Sturm, R. Schmidt-Grund, M. Grundmann, *Sci. Rep.* **2016**, *6*, 35964.

© 2020 The Authors. Published by WILEY-VCH Verlag GmbH & Co. KGaA, Weinheim

Bibliography

[Age11] Agency, International Energy: *World Energy Outlook 2011.* Organization for Economic, 2011 (cit. on p. 1).

[Åhm96] Åhman, J., G. Svensson, and J. Albertsson: 'A reinvestigation of β-gallium oxide'. *Acta Crystallographica Section C: Crystal Structure Communications* (1996), vol. 52(6): pp. 1336–1338. doi: 10.1107/S0108270195016404 (cit. on pp. 7, 10).

[Aid08] Aida, H., K. Nishiguchi, H. Takeda, N. Aota, K. Sunakawa, and Y. Yaguchi: 'Growth of β-Ga_2O_3 Single Crystals by the Edge-Defined, Film Fed Growth Method'. *Japanese Journal of Applied Physics* (2008), vol. 47(11): pp. 8506–8509. doi: 10.1143/jjap.47.8506 (cit. on p. 7).

[Aid14] Aida, R., K. Minami, K. Ishibashi, J. Kudou, M. Takahara, I. Tsunoda, K. Takakura, T. Nakashima, M. Shibuya, and K. Murakami: 'Effect of post-deposition annealing on structural and optical properties of RF magnetron sputtered β-Ga_2O_3 films'. *AIP Conference Proceedings.* Vol. 1583. 1. AIP. 2014: pp. 364–367. doi: 10.1063/1.4865671 (cit. on p. 7).

[And10] Anders, A.: 'A structure zone diagram including plasma-based deposition and ion etching'. *Thin Solid Films* (2010), vol. 518(15): pp. 4087–4090. doi: 10.1016/j.tsf.2009.10.145 (cit. on pp. 12, 13).

[Bag15] Bagher, A. M, M. M. A. Vahid, and M. Mohsen: 'Types of Solar Cells and Application'. *American Journal of Optics and Photonics* (2015), vol. 3(5): pp. 94–113. doi: 10.11648/j.ajop.20150305.17 (cit. on p. 3).

[Bat96] Battiston, G. A., R. Gerbasi, M. Porchia, R. Bertoncello, and F. Caccavale: 'Chemical vapour deposition and characterization of gallium oxide thin films'. *Thin Solid Films* (1996), vol. 279(1-2): pp. 115–118. doi: 10.1016/0040-6090(95)08161-5 (cit. on p. 7).

[Bec20] Becker, M., S.L. Benz, L. Chen, A. Polity, P.J. Klar, and S. Chatterjee: 'Controlled thin-film deposition of α or β Ga_2O_3 by ion-beam sputtering'. *J. Vac. Sci. Technol. A* (2020), vol. 38: p. 063412. doi: 10.1088/0022-3727/46/20/205205 (cit. on p. 22).

[Ben] Benz, S.L., M. Becker, A. Polity, P.J. Klar, and S. Chatterjee: 'Determining the band alignment of copper-oxide gallium-oxide heterostructures'. (Cit. on p. 22).

[Ber18a] Berger, Roland, ed.: *Megatrend 3: Scarcity of Resources*. 2018 (cit. on p. 3).

[Ber18b] Berger, Roland, ed.: *Megatrend 7: Sustainability & Global Responsibility*. 2018 (cit. on p. 3).

[Bra14] Brandt, R. E., M. Young, H. H. Park, A. Dameron, D. Chua, Y. Seog Lee, G. Teeter, R. G. Gordon, and T. Buonassisi: 'Band offsets of n-type electron-selective contacts on cuprous oxide (Cu_2O) for photovoltaics'. *Applied Physics Letters* (2014), vol. 105(26): p. 263901. doi: 10.1063/1.4905180 (cit. on pp. 2, 4, 5).

[Čap13] Čapek, J., M. Hála, O. Zabeida, J.E. Klemberg-Sapieha, and L. Martinu: 'Deposition rate enhancement in HiPIMS without compromising the ionized fraction of the deposition flux'. *J. Phys. D: Appl. Phys.* (2013), vol. 46(20): p. 205205. doi: 10.1088/0022-3727/46/20/205205 (cit. on p. 12).

[Cho02] Choopun, S., R. D. Vispute, W. Yang, R. P. Sharma, T. Venkatesan, and H. Shen: 'Realization of band gap above 5.0 eV in metastable cubic-phase $Mg_xZn_{1-x}O$ alloy films'. *Applied Physics Letters* (2002), vol. 80(9): pp. 1529–1531. doi: 10.1063/1.1456266 (cit. on p. 5).

[Com17] Commission, European: *Methodology for establishing the EU list of critical raw materials*. Tech. rep. Directorate-General for Internal Market, Industry, Entrepreneurship and SMEs (European Commission), 2017. doi: 10.2873/769526 (cit. on pp. 1, 4, 5).

[Com20] Commission, European: *Study on the EU's list of Critical Raw Materials (2020), Factsheets on Critical Raw Materials*. Tech. rep. Directorate-General for Internal Market, Industry, Entrepreneurship and SMEs (European Commission), 2020. doi: 10.2873/92480 (cit. on pp. 1, 4, 5).

[Del17] Deloitte, Consulting GmbH: *Beyond the Noise - The Megatrends of Tomorrow's World*. Vol. 1. LOGOPUBLIX Fachbuch Verlag, München, 2017 (cit. on p. 3).

[Die09] Diederen, A.: 'Metal minerals scarcity: A call for managed austerity and the elements of hope'. *TNO Defence, Security and Safety* (2009), vol. (cit. on p. 2).

[Don16] DONG, L., R. JIA, B. XIN, and Y. ZHANG: 'Effects of post-annealing temperature and oxygen concentration during sputtering on the structural and optical properties of β-Ga_2O_3 films'. *Journal of Vacuum Science & Technology A: Vacuum, Surfaces, and Films* (2016), vol. 34(6): p. 060602. DOI: 10.1116/1.4963376 (cit. on p. 7).

[Fen16] FENG, X., Z. LI, W. MI, and J. MA: 'Effect of annealing on the properties of Ga_2O_3:Mg films prepared on α-Al_2O_3(0001) by MOCVD'. *Vacuum* (2016), vol. 124: pp. 101–107. DOI: 10.1016/j.vacuum.2015.06.032 (cit. on p. 7).

[Fon10] FONASH, S.: *Solar Cell Device Physics*. Vol. 2. Elsevier Science & Technology, Apr. 11, 2010. 400 pp. (cit. on pp. 1, 4, 5).

[Gal18] GALAZKA, Z.: 'β-Ga_2O_3 for wide-bandgap electronics and optoelectronics'. *Semicond. Sci. Technol.* (2018), vol. 33(11): p. 113001. DOI: 10.1088/1361-6641/aadf78 (cit. on pp. 1, 7).

[Gal10] GALAZKA, Z., R. UECKER, K. IRMSCHER, M. ALBRECHT, D. KLIMM, M. PIETSCH, M. BRÜTZAM, R. BERTRAM, S. GANSCHOW, and R. FORNARI: 'Czochralski growth and characterization of β-Ga2O3 single crystals'. *Crystal Research and Technology* (2010), vol. 45(12): pp. 1229–1236. DOI: 10.1002/crat.201000341 (cit. on pp. 7, 9).

[Gar16] GARCÍA-VALENZUELA, J.A., R. RIVERA, A.B. MORALES-VILCHES, L.G. GERLING, A. CABALLERO, J.M. ASENSI, C. VOZ, J. BERTOMEU, and J. ANDREU: 'Main properties of Al_2O_3 thin films deposited by magnetron sputtering of an Al_2O_3 ceramic target at different radio-frequency power and argon pressure and their passivation effect on p-typce c-Si wafers'. *Thin Solid Films* (2016), vol. 619: pp. 288–296. DOI: 10.1016/j.tsf.2016.10.049 (cit. on p. 17).

[Gru91] GRUEN, R.: 'Process and apparatus for coating conducting pieces using a pulsed glow discharge'. 5015493A (US). 1991 (cit. on p. 12).

[Guo15] GUO, Z., A. VERMA, X. WU, F. SUN, A. HICKMAN, T. MASUI, A. KURAMATA, M. HIGASHIWAKI, D. JENA, and T. LUO: 'Anisotropic thermal conductivity in single crystal β-gallium oxide'. *Applied Physics Letters* (2015), vol. 106(11): p. 111909. DOI: 10.1063/1.4916078 (cit. on p. 8).

[Hig18] HIGASHIWAKI, M. and G. H. JESSEN: 'Guest Editorial: The dawn of gallium oxide microelectronics'. *Applied Physics Letters* (2018), vol. 112(6): p. 060401. DOI: 10.1063/1.5017845 (cit. on p. 1).

[Hig16a] Higashiwaki, M., H. Murakami, Y. Kumagai, and A. Kuramata: 'Current status of Ga_2O_3 power devices'. *Japanese Journal of Applied Physics* (2016), vol. 55(12): 1202A1. doi: 10.7567/jjap.55.1202a1 (cit. on p. 1).

[Hig16b] Higashiwaki, M., K. Sasaki, H Murakami, Y. Kumagai, A. Koukitu, A. Kuramata, T. Masui, and S. Yamahoshi: 'Recent progress in Ga_2O_3 power devices'. *Semicond. Sci. Technol.* (2016), vol. 31(3): p. 034001. doi: 10.1088/0268-1242/31/3/034001 (cit. on p. 1).

[Hof94] Hoffman, D. W.: 'Perspective on stresses in magnetron-sputtered thin films'. *J. Vac. Sci. Technol. A* (1994), vol. 12(4): p. 953. doi: 10.1116/1.579073 (cit. on p. 12).

[Irm11] Irmscher, K., Z. Galazka, M. Pietsch, R. Uecker, and R. Fornari: 'Electrical properties of β-Ga_2O_3 single crystals grown by the Czochralski method'. *Journal of Applied Physics* (2011), vol. 110(6): p. 063720. doi: 10.1063/1.3642962 (cit. on p. 7).

[Jan11] Janowitz, ., V. Scherer, M. Mohamed, A. Krapf, H. Dwelk, R. Manzke, Z. Galazka, R. Uecker, K. Irmscher, R. Fornari, M. Michling, D. Schmeisser, J. R. Weber, J. B. Varley, and C. G Van de Walle: 'Experimental electronic structure of In_2O_3 and Ga_2O_3'. *New Journal of Physics* (2011), vol. 13(8): p. 085014. doi: 10.1088/1367-2630/13/8/085014 (cit. on pp. 9, 10).

[Kel09] Kelly, P. J. and J. W. Bradley: 'Pulsed magnetron sputtering - process overview and applications'. *Journal of optoelectronics and advanced materials* (2009), vol. 11(9): pp. 1101–1107. doi: 10.1063/1.4864283 (cit. on pp. 2, 12).

[Kel78] Kelly, R.: 'An attempt to understand preferential sputtering'. *Nuclear Instruments and Methods* (1978), vol. 149(1-3): pp. 553–558. doi: 10.1016/0029-554x(78)90925-4 (cit. on pp. 5, 15).

[KPM14] KPMG, International Cooperative: *Future State 2030: The global megatrends shaping governments*. 2014 (cit. on p. 3).

[Kra12] Kramm, B., A. Laufer, D. Reppin, A. Kronenberger, P. Hering, A. Polity, and B. K. Meyer: 'The band alignment of Cu2O/ZnO and Cu2O/GaN heterostructures'. *Applied Physics Letters* (2012), vol. 100(9): p. 094102. doi: 10.1063/1.3685719 (cit. on pp. 4, 5).

[Kra16] Kranert, C., C. Sturm, R. Schmidt-Grund, and M. Grundmann: 'Raman tensor elements of β-Ga_2O_3'. *Scientific Reports* (2016), vol. 6(1). doi: 10.1038/srep35964 (cit. on p. 8).

[Kro13] Kronenberger, A.: 'Herstellung und Charakterisierung von $ZnO_{1-x}S_x$-Dünnschichten'. PhD thesis. Justus-Liebig-University Giessen, Germany, 2013 (cit. on p. 4).

[Kru18] Kruamata, A., K. Koshi, S. Watanabe, Y. Yamaoka, T. Masui, and S. Yamakoshi: 'Bulk crystal growth of Ga_2O_3'. *Proc. SPIE, Oxide-based Materials and Devices IX* (2018), vol. 10533(105330E). doi: 10.1117/12.2301405 (cit. on p. 7).

[Kum13] Kumar, S. S., E. J. Rubio, M. Noor-A-Alam, G. Martinez, S. Manandhar, V. Shutthanandan, S. Thevuthasan, and C. V. Ramana: 'Structure, Morphology, and Optical Properties of Amorphous and Nanocrystalline Gallium Oxide Thin Films'. *The Journal of Physical Chemistry C* (2013), vol. 117(8): pp. 4194–4200. doi: 10.1021/jp311300e (cit. on pp. 2, 18).

[Kyr18] Kyrtsos, Alexandros, Masahiko Matsubara, and Enrico Bellotti: 'On the feasibility of p-type Ga2O3'. *Applied Physics Letters* (2018), vol. 112(3): p. 032108. doi: 10.1063/1.5009423 (cit. on p. 9).

[Lan18] Lany, Stephan: 'Defect phase diagram for doping of Ga2O3'. *APL Materials* (2018), vol. 6(4): p. 046103. doi: 10.1063/1.5019938 (cit. on p. 9).

[Mar12] Marwoto, P., S. Sugianto, and E. Wibowo: 'Growth of europium-doped gallium oxide (Ga_2O_3:Eu) thin films deposited by homemade DC magnetron sputtering'. *Journal of Theoretical and Applied Physics* (2012), vol. 6(1): p. 17. doi: 10.1186/2251-7235-6-17 (cit. on p. 7).

[Mat06] Matsuzaki, K., H. Hiramatsu, K. Nomura, H. Yanagi, T. Kamiya, M. Hirano, and H. Hosono: 'Growth, structure and carrier transport properties of Ga_2O_3 epitaxial film examined for transparent field-effect transistor'. *Thin Solid Films* (2006), vol. 496(1): pp. 37–41. doi: 10.1016/j.tsf.2005.08.187 (cit. on p. 7).

[Mey12] Meyer, B. K. et al.: 'Binary copper oxide semiconductors: From materials towards devices'. *physica status solidi (b)* (2012), vol. 249(8): pp. 1487–1509. doi: 10.1002/pssb.201248128 (cit. on pp. 1, 4).

[Min03] Minami, T.: 'Oxide thin-film electroluminescent devices and materials'. *Solid-State Electronics* (2003), vol. 47(12): pp. 2237–2243. doi: 10.1016/s0038-1101(03)00204-1 (cit. on p. 7).

[Min13a] Minami, T., Y. Nishi, and T. Miyata: 'Effect of the thin Ga_2O_3 layer in n+-ZnO/n-Ga_2O_3/p-Cu_2O heterojunction solar cells'. *Thin Solid Films* (2013), vol. 549: pp. 65–69. doi: 10.1016/j.tsf.2013.06.038 (cit. on p. 5).

[Min13b] Minami, T., Y. Nishi, and T. Miyata: 'High-Efficiency Cu_2O-Based Heterojunction Solar Cells Fabricated Using a Ga_2O_3 Thin Film as N-Type Layer'. *Applied Physics Express* (2013), vol. 6(4): p. 044101. doi: 10.7567/apex.6.044101 (cit. on pp. 2, 5, 7).

[Min00] Minemoto, T., T. Negami, S. Nishiwaki, H. Takakura, and Y. Hamakawa: 'Preparation of $Zn_{1-x}Mg_xO$ films by radio frequency magnetron sputtering'. *Thin Solid Films* (2000), vol. 372(1-2): pp. 173–176. doi: 10.1016/s0040-6090(00)01009-9 (cit. on p. 5).

[Moo11] Moos, R., N. Izu, F. Rettig, S. Reiss, W. Shin, and I. Matsubara: 'Resistive Oxygen Gas Sensors for Harsh Environments'. *Sensors* (2011), vol. 11(4): pp. 3439–3465. doi: 10.3390/s110403439 (cit. on p. 7).

[Nak12] Nakagomi, S. and Y. Kokubun: 'Crystal orientation of β-Ga_2O_3 thin films formed on c-plane and a-plane sapphire substrate'. *Journal of Crystal Growth* (2012), vol. 349(1): pp. 12–18. doi: 10.1016/j.jcrysgro.2012.04.006 (cit. on p. 18).

[Nak14] Nakamura, E., K. Ueno, J. Ohta, H. Fujioka, and M. Oshima: 'Dramatic reduction in process temperature of InGaN-based light-emitting diodes by pulsed sputtering growth technique'. *Applied Physics Letters* (2014), vol. 104(4): p. 051121. doi: 10.1063/1.4864283 (cit. on p. 12).

[Nat01] Nations, United and United Nations Development Programme: *World Energy Assessment: Energy and the Challenge of Sustainability.* United Nations, 2001 (cit. on p. 1).

[Oht98] Ohtomo, A., M. Kawasaki, T. Koida, K. Masubuchi, H. Koinuma, Y. Sakurai, Y. Yoshida, T. Yasuda, and Y. Segawa: '$Mg_xZn_{1-x}O$ as a II–VI widegap semiconductor alloy'. *Applied Physics Letters* (1998), vol. 72(19): pp. 2466–2468. doi: 10.1063/1.121384 (cit. on p. 5).

[Oku14] Okumura, H., M. Kita, K. Sasaki, A. Kuramata, M. Higashiwaki, and J. S. Speck: 'Systematic investigation of the growth rate of β-Ga_2O_3(010) by plasma-assisted molecular beam epitaxy'. *Applied Physics Express* (2014), vol. 7(9): p. 095501. doi: 10.7567/apex.7.095501 (cit. on p. 7).

[Onu13] Onuma, T., S. Fujioka, T. Yamaguchi, M. Higashiwaki, K. Sasaki, T. Masui, and T. Honda: 'Correlation between blue luminescence intensity and resistivity in β-Ga_2O_3 single crystals'. *Applied Physics Letters* (2013), vol. 103(4): p. 041910. doi: 10.1063/1.4816759 (cit. on p. 9).

[Ori02] Orita, M., H. Hiramatsu, H. Ohta, M. Hirano, and H. Hosono: 'Preparation of highly conductive, deep ultraviolet transparent β-Ga_2O_3 thin film at low deposition temperatures'. *Thin Solid Films* (2002), vol. 411(1): pp. 134–139. doi: 10.1016/s0040-6090(02)00202-x (cit. on p. 18).

[Ori00] Orita, M., H. Ohta, M. Hirano, and H. Hosono: 'Deep-ultraviolet transparent conductive β-Ga_2O_3 thin films'. *Applied Physics Letters* (2000), vol. 77(25): pp. 4166–4168. doi: 10.1063/1.1330559 (cit. on pp. 1, 9).

[Osh07] Oshima, T., T. Okuno, and S. Fujita: 'Ga_2O_3 Thin Film Growth on c-Plane Sapphire Substrates by Molecular Beam Epitaxy for Deep-Ultraviolet Photodetectors'. *Japanese Journal of Applied Physics* (2007), vol. 46(11): pp. 7217–7220. doi: 10.1143/jjap.46.7217 (cit. on pp. 7, 18).

[Par01] Park, W. I., Gyu-Chul Yi, and H. M. Jang: 'Metalorganic vapor-phase epitaxial growth and photoluminescent properties of $Zn_{1-x}Mg_xO$ ($0 \leqslant x \leqslant 0.49$) thin films'. *Applied Physics Letters* (2001), vol. 79(13): pp. 2022–2024. doi: 10.1063/1.1405811 (cit. on p. 5).

[Pas95] Passlack, M., E. F. Schubert, W. S. Hobson, M. Hong, N. Moriya, S. N. G. Chu, K. Konstadinidis, J. P. Mannaerts, M. L. Schnoes, and G. J. Zydzik: 'Ga_2O_3 films for electronic and optoelectronic applications'. *Journal of Applied Physics* (1995), vol. 77(2): pp. 686–693. doi: 10.1063/1.359055 (cit. on p. 10).

[Pea18] Pearton, S. J., Jiancheng Yang, Patrick H. Cary, F. Ren, Jihyun Kim, Marko J. Tadjer, and Michael A. Mastro: 'A review of Ga_2O_3 materials, processing, and devices'. *Applied Physics Reviews* (2018), vol. 5(1): p. 011301. doi: 10.1063/1.5006941 (cit. on pp. 2, 7).

[Pee15] Peelaers, H. and C. G. Van de Walle: 'Brillouin zone and band structure of β-Ga_2O_3'. *physica status solidi (b)* (2015), vol. 252(4): pp. 828–832. doi: 10.1002/pssb.201451551 (cit. on p. 9).

[Pos95] Posadowski, W. M.: 'Sustained self sputtering of different materials using dc magnetron'. *Vacuum* (1995), vol. 46(8–10): pp. 1017–1020. doi: 10.1016/0042-207X(95)00096-8 (cit. on p. 12).

[Raf17] Rafique, S., L. Han, S. Mou, and H. Zhao: 'Temperature and doping concentration dependence of the energy band gap in β-Ga_2O_3 thin films grown on sapphire'. *Optical Materials Express* (2017), vol. 7(10): p. 3561. doi: 10.1364/ome.7.003561 (cit. on p. 9).

[Ram14] Ramana, C. V., E. J. Rubio, C. D. Barraza, A. M. Gallardo, S. McPeak, S. Kotru, and J. T. Grant: 'Chemical bonding, optical constants, and electrical resistivity of sputter-deposited gallium oxide thin films'. *Journal of Applied Physics* (2014), vol. 115(4): p. 043508. doi: 10.1063/1.4862186 (cit. on p. 2).

[Reb02] Rebien, M., W. Henrion, M. Hong, J. P. Mannaerts, and M. Fleischer: 'Optical properties of gallium oxide thin films'. *Applied Physics Letters* (2002), vol. 81(2): pp. 250–252. doi: 10.1063/1.1491613 (cit. on pp. 7, 16).

[Roe67] Roessler, D. M. and W. C. Walker: 'Electronic Spectrum and Ultraviolet Optical Properties of Crystalline MgO'. *Physical Review* (1967), vol. 159(3): pp. 733–738. doi: 10.1103/physrev.159.733 (cit. on p. 4).

[Roy52] Roy, R., V.G. Hill, and E.F. Osborn: 'Polymorphism of Ga_2O_3 and the System Ga_2O_3-H_2O'. *Journal of the American Chemical Society* (1952), vol. 74(3): pp. 719–722. doi: 10.1021/ja01123a039 (cit. on pp. 7, 8).

[Sal06] Salmang, H. and H. Scholze: *Keramik*. Springer Berlin Heidelberg, Nov. 25, 2006 (cit. on p. 15).

[Sar10] Sarakinos, K., J. Alami, and S. Konstantinidis: 'High power pulsed magnetron sputtering: A review on scientific and engineering state of the art'. *Surface & Coatings Technology* (2010), vol. 204(204): pp. 1661–1684. doi: 10.1016/j.surfcoat.2009.11.013 (cit. on pp. 2, 12).

[Sar59] Sarver, J. F., Fred L. Katnack, and F. A. Hummel: 'Phase Equilibria and Manganese-Activated Fluorescence in the System $Zn_3(PO_4)_2$-$Mg_3(PO_4)_2$'. *Journal of The Electrochemical Society* (1959), vol. 106(11): p. 960. doi: 10.1149/1.2427190 (cit. on p. 5).

[Sch63] Schneider, S.J. and J.L. Waring: 'Phase equilibrium relations in the Sc_2O_3-Ga_2O_3 system'. *J. Res. Natl. Bur. Std.* (1963), vol. 67A: pp. 19–25. doi: 10.6028/jres.067A.003 (cit. on p. 10).

[Sch19] Schurig, P., M. Couturier, M. Becker, A. Polity, and P.J. Klar: 'Optimizing the Stoichiometry of Ga_2O_3 Grown by RF-Magnetron Sputter Deposition by Correlating Optical Properties and Growth Parameters'. *Phys. Status Solidi A* (2019), vol. 216(20): p. 1900385. doi: 10.1002/pssa.201900385 (cit. on p. 23).

[Sch20] Schurig, P., F. Michel, A. Beyer, K. Volz, M. Becker, A. Polity, and P.J. Klar: 'Progress in Sputter Growth of β-Ga_2O_3 by Applying Pulsed-Mode Operation'. *Phys. Status Solidi A* (2020), vol. 217(10): p. 1901009. doi: 10.1002/pssa.201901009 (cit. on p. 30).

[Seg65] SEGNIT, E. R. and A. E. HOLLAND: 'The System MgO-ZnO-SiO_2'. *Journal of the American Ceramic Society* (1965), vol. 48(8): pp. 409–413. DOI: 10.1111/j.1151-2916.1965.tb14778.x (cit. on p. 5).

[Sha09] SHAFIEE, S. and E. TOPAL: 'When will fossil fuel reserves be diminished?' *Energy Policy* (2009), vol. 37(1): pp. 181–189. DOI: 10.1016/j.enpol.2008.08.016 (cit. on p. 1).

[Sho61] SHOCKLEY, W. and H. J. QUEISSER: 'Detailed Balance Limit of Efficiency of p-n Junction Solar Cells'. *Journal of Applied Physics* (1961), vol. 32(3): pp. 510–519. DOI: 10.1063/1.1736034 (cit. on p. 1).

[Sho14] SHON, J. W., J. OHTA, K. UENO, A. KOBAYASHI, and H. FUJIOKA: 'Fabrication of full-color InGaN-based light-emitting diodes on amorphous substrates by pulsed sputtering'. *Scientific Reports* (2014), vol. 4: p. 4325. DOI: 10.1038/sreo05325 (cit. on p. 12).

[Ste16] STEPANOV, S.I., V.I. NIKOLAEV, V.E. BOUGROV, and A.E. ROMANOV: 'Gallium oxide: properties and applications - a review'. *Reviews on advanced materials science* (2016), vol. 44: pp. 63–86 (cit. on pp. 2, 7–9).

[Sun02] SUN, H. D., T. MAKINO, Y. SEGAWA, M. KAWASAKI, A. OHTOMO, K. TAMURA, and H. KOINUMA: 'Enhancement of exciton binding energies in ZnO/ZnMgO multiquantum wells'. *Journal of Applied Physics* (2002), vol. 91(4): pp. 1993–1997. DOI: 10.1063/1.1445280 (cit. on p. 5).

[Tho89] THORNTON, J. A. and D. W. HOFFMAN: 'Stress-related effects in thin films'. *Thin Solid Films* (1989), vol. 171(1): pp. 5–31. DOI: 10.1016/0040-6090(89)90030-8 (cit. on p. 12).

[Tol17] TOLSTOVA, Y., S. T. OMELCHENKO, R. E. BLACKWELL, A.M. SHING, and H. A. ATWATER: 'Polycrystalline Cu2O photovoltaic devices incorporating Zn(O,S) window layers'. *Solar Energy Materials and Solar Cells* (2017), vol. 160: pp. 340–345. DOI: 10.1016/j.solmat.2016.10.049 (cit. on p. 4).

[Ued97] UEDA, N., H. HOSONO, R. WASEDA, and H. KAWAZOE: 'Synthesis and control of conductivity of ultraviolet transmitting β-Ga_2O_3 single crystals'. *Applied Physics Letters* (1997), vol. 70(26): pp. 3561–3563. DOI: 10.1063/1.119233 (cit. on pp. 8, 9).

[Var12] VARLEY, J. B., A. JANOTTI, C. FRANCHINI, and C. G. VAN de WALLE: 'Role of self-trapping in luminescence and p-type conductivity of wide-band-gap oxides'. *Physical Review B* (2012), vol. 85(8). DOI: 10.1103/physrevb.85.081109 (cit. on p. 9).

[Var10] Varley, J. B., J. R. Weber, A. Janotti, and C. G. Van de Walle: 'Oxygen vacancies and donor impurities in β-Ga_2O_3'. *Applied Physics Letters* (2010), vol. 97(14): p. 142106. doi: 10.1063/1.3499306 (cit. on pp. 9, 10).

[Vil06] Villora, E. G., K. Shimamura, K. Kitamura, and . Aoki: 'Rf-plasma-assisted molecular-beam epitaxy of β-Ga_2O_3'. *Applied Physics Letters* (2006), vol. 88(3): p. 031105. doi: 10.1063/1.2164407 (cit. on p. 7).

[Vil08] Villora, E.G., K. Shimamura, Y. Yoshikawa, T. Ujiie, and K. Aoki: 'Electrical conductivity and carrier concentration control in β-Ga_2O_3 by Si doping'. *Applied Physics Letters* (2008), vol. 92(20): p. 202120. doi: 10.1063/1.2919728 (cit. on p. 10).

[Vog16] Vogt, P. and O. Bierwagen: 'Comparison of the growth kinetics of In_2O_3 and Ga_2O_3 and their suboxide desorption during plasma-assisted molecular beam epitaxy'. *Applied Physics Letters* (2016), vol. 109(6): p. 062103. doi: 10.1063/1.4960633 (cit. on p. 7).

[Wen17] Wenckstern, H. von: 'Group-III Sesquioxides: Growth, Physical Properties and Devices'. *Advanced Electronic Materials* (2017), vol. 3(9): p. 1600350. doi: 10.1002/aelm.201600350 (cit. on pp. 7, 9).

[Yam04] Yamaguchi, K.: 'First principles study on electronic structure of β-Ga_2O_3'. *Solid State Communications* (2004), vol. 131(12): pp. 739–744. doi: 10.1016/j.ssc.2004.07.030 (cit. on p. 9).

[Yos07] Yoshioka, S., H. Hayashi, A. Kuwabara, F. Oba, K. Matsunaga, and I. Tanaka: 'Structures and energetics of Ga_2O_3 polymorphs'. *Journal of Physics: Condensed Matter* (2007), vol. 19(34): p. 346211. doi: 10.1088/0953-8984/19/34/346211 (cit. on p. 9).

[Zha14] Zhang, F. B., K. Saito, T. Tanaka, M. Nishio, and Q. X. Guo: 'Structural and optical properties of Ga_2O_3 films on sapphire substrates by pulsed laser deposition'. *Journal of Crystal Growth* (2014), vol. 387: pp. 96–100. doi: 10.1016/j.jcrysgro.2013.11.022 (cit. on p. 7).

[Zha18] Zhang, F., H. Li, Y.-T. Cui, G.-L. Li, and Q. Guo: 'Evolution of optical properties and band structure from amorphous to crystalline Ga_2O_3 films'. *AIP Advances* (2018), vol. 8(4): p. 045112. doi: 10.1063/1.5021867 (cit. on p. 18).

[Zin04] Zinkevich, M. and F. Aldinger: 'Thermodynamic Assessment of the Gallium-Oxygen System'. *Journal of the American Ceramic Society* (2004), vol. 87(4): pp. 683–691. doi: 10.1111/j.1551-2916.2004.00683.x (cit. on p. 1).

A ZnMgO(:Al)

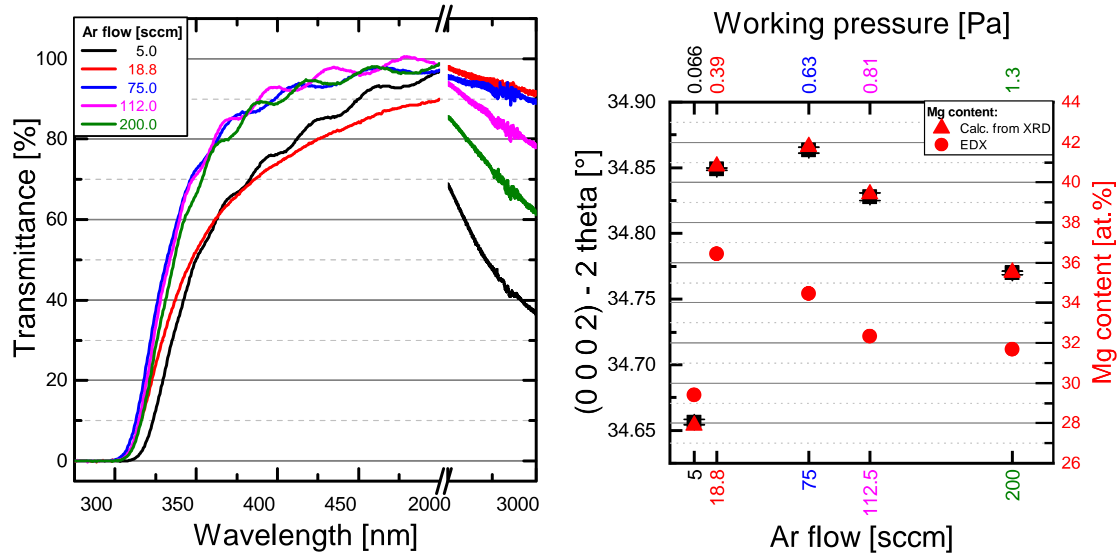

(a) Transmittance results of ZnMgOAl layers deposited at different Ar flows. The spectra show the spectral ranges in the vicinity of the absorption edge and of the free-carrier induced absorption. A dependence of the transmittance value on the Mg content seems to occur.

(b) 2 Theta values (squares) of (0002) reflection obtained from layers deposited at different Ar flows and calculated Mg content (triangles) as well as EDX results (circles). The EDX results show the real development of Mg content which is in accordance with the change in transmittance in (a).

Figure A.1: Transmittance (a), 2 theta position and Mg content (b) of layers deposited at various Ar flows from the same $Zn_{0.72}Mg_{0.25}O{:}Al_{0.03}$ target.

B Annealing Ga_2O_3

The post deposition temperature treatment was conducted as a rapid thermal annealing (RTA) process at 1000 °C for 2 h under ambient atmosphere. This treatment condition was found to lead to an increased optical band gap, presumably due to Al diffusion from the substrate into the deposited layer.

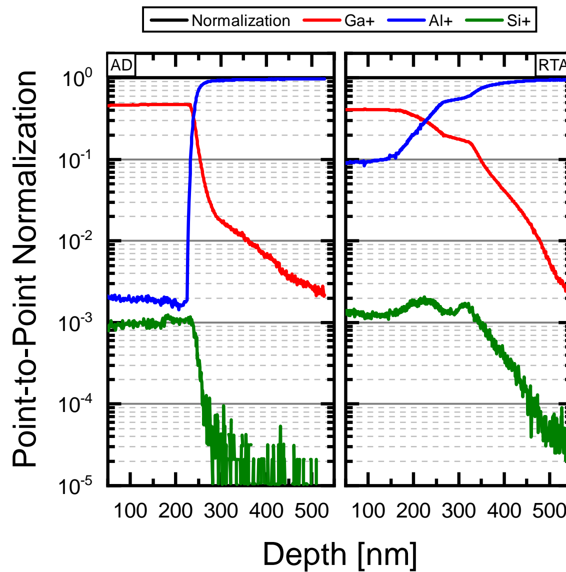

Fig. B.1: time of flight secondary-ion mass spectrometry (ToF-SIMS) depth profiles of Ga_2O_3 layer deposited with 400 W from the commercial target onto *c*-plane sapphire.

Consequently ToF-SIMS depth profiles of as-deposited (AD) and rapid thermal annealed (RTA) samples were measured to investigate the element distribution throughout the grown Ga_2O_3 layer and at the substrate interface. The results are illustrated again with point-to-point normalization. Utilizing this method the change of the sputter matrix effects, e. g. different sputtering yields for layer and substrate, are normalized. Thus, weak signals get slightly overpronounced and one has to be careful in the interpretation. In the AD case (Fig. B.1, left) a sharp transition between the layer and the substrate is present, although the Ga signal extends deeper into the substrate which can partly be accounted to the method used. During removing of the material by ion bombardment it is inevitable that some of the material of the top layer will intermix with the underlying layers induced by the particle collisions. Furthermore, Si and Al were detected within the Ga_2O_3 layer with roughly the same normalized intensity. Because of missing relative sensitivity factors (RSFs) the results cannot be quantified, but might serve as a trend. Additionally one has to keep in mind that although the intensities exhibit the same counts, the actual concentrations are different as the RSF of each element is different. Therefore, one can conclude qualitatively that with reaching the substrate two out of three elements

vanish. Nevertheless, the presence of the three elements is reasonable because Si is the main impurity in Ga_2O_3 targets. After annealing (Fig. B.1, right) the interface region is much more broadened than before. The Al signal within the layer is two magnitudes higher and a strong indication for a pronounced diffusion of Al from the substrate into the layer. This confirms the increased optical band gap of the deposited layer after annealing. Likewise the Ga signal gets more pronounced within the substrate because of diffusion. Care has to be taken in the intermediate region of the depth profile. In this range the element matrix changes with every sputtering step for elemental analysis. Additionally some normally weak details, e. g. the hill-like increase in the Si signal, can be overestimated due to the changing sputtering matrix or the point-to-point normalization.

In summary, the ToF-SIMS results strongly indicate that the annealing process triggers an intense diffusion of Al or Ga into the layer or substrate, respectively. Moreover the interface region is no longer distinct after annealing.

Declaration

I declare that I have completed this dissertation single-handedly without the unauthorized help of a second party and only with the assistance acknowledged therein. I have appropriately acknowledged and cited all text passages that are derived verbatim from or are based on the content of published work of others, and all information relating to verbal communications. I consent to the use of an anti-plagiarism software to check my thesis. I have abided by the principles of good scientific conduct laid down in the charter of the Justus Liebig University Giessen „Satzung der Justus-Liebig-Universität Gießen zur Sicherung guter wissenschaftlicher Praxis“ in carrying out the investigations described in the dissertation.

<February 25, 2021, Linden> <Philipp Schurig>